Application of Acoustic Micro Tomographic Techniques to the Study of Variability of Physical Property of Water Mass

（水塊変動研究へのマイクロトモグラフィ技術の応用）

August, 1992

Toshiharu KAWASAKI

Application of Acoustic Micro Tomographic Techniques to the Study of Variability of Physical Property of Water Mass

by

Toshiharu KAKIHARA

Tokyo University of Fisheries

A Dissertation Presented to
The Faculty of Science
University of Tokyo

In Partial Fulfillment of the Requirements
for the Degree of
Doctor of Science

August, 1992

Abstract

A new method to estimate the vertical structure of sound speed and/or temperature using the acoustic micro tomographic technique was developed. Experiments were carried out to verify the effectiveness of the acoustic micro tomographic techniques to study the variability of physical properties of water mass of local area in a small scale, i.e., a few kilometer range. From the results of expriment in the Sagami Bay the feasibility of microtomography was confirmed. The method proposed in this study proved to be useful in the target area for monitoring mean sound speed structure which varies with seasons, oceanic current and so on.

The data of propagation time of acoustic signals which propagate directly between the acoustic transponders installed at the sea surface and at the sea floor are used in this method. The mean profile of vertical sound speed is estimated inversely from the measured propagation time by employing the least squares method to obtain optimum coefficients of sound speed function expressed by the Chebychev polynomial.

The experiments were carried out twice in the Sagami Bay. The first experiment conducted in 1991 was a preliminary one, from which we learned several problems to be solved. The second experiment in 1992 was conducted to verify the plausibility of the microtomography, and some results significant to oceanography and /or fisheries were obtained.

The results obtained from 1992 experiment show that the estimation accuracy of sound speed profile was about -0.46m/sec on an average and 1.11m/sec in standard deviation throughout the depth from the surface to 1400m. This corresponds to -0.15 °C on an average and 0.31 °C in standard deviation.

In addition, the estimation method of mean temperature using propagation time data as indices of oceanic variability in the shallow layer is discussed and the practical transponder network to realize microtomographic researches is also dealt with in this study. It has been concluded that the study of ocean acoustic microtomography should contribute to the coastal oceanography and the fisheries.

Résumé

On a étudié une nouvelle méthode de l'estimation, à l'aide de la technique microtomographique acoustique, de la structure verticale de la vitesse sonique et/ou de la température dans l'eau de mer. Des expériences ont été effectuées pour vérifier l'efficacité de la technique microtomographique acoustique dans les études de la variabilité à micro-échelle, à l'échelle de quelques kilomètres, des propriétés physiques de la masse d'eau d'une zone locale. A partir des résultats obtenus dans le Golfe de Sagami, la faisabilité de la microtomographie s'est confirmée. Il a été démontré que la méthode proposée dans cette étude serait utile dans une zone visée, pour surveiller la structure moyenne de la vitesse sonique qui varie avec les saisons, les courants marins, et avec d'autres paramètres.

On utilise dans cette méthode les données rélatives au temps de propagation des signaux acoustiques qui se propagent directement entre les transpondeurs installés à la surface marine et au fond océanique. Il est estimé le profil moyen de la vitesse sonique, inversement à partir des temps de propagation mesurés, au moyen de la méthode de moindres carrés par laquelle s'obtiennent les coefficients optima de la fonction de la vitesse sonique exprimés par le polynôme de Chebychev.
L'exactitude de l'estimation à l'égard du profil de la vitesse sonique était d'en moyenne de -0,46m/sec avec un écart standard de 1,11m/sec, au travers de la profondeur de 1.400 m de la surface. Cette exactitude correspond à une température moyenne de -0,15°C avec un écart standard de 0,31°C.

On discute la méthode de l'estimation de la température à l'aide des données rélatives au temps en tant qu'indices de la variabilité de l'eau de mer en couches moins profondes, et traite également les problèmes vis-à-vis de la mise en oeuvre du réseau transpondeur pratique envisagé pour réaliser les recherches microtomographiques.

Il en est conclu que l'étude de la microtomographie acoustique océanique devrait contribuer à l'océanographie et à la pêche côtières.

Acknowledgements

First of all, I would like to express my cordial gratitude to Professor Dr. J. Segawa for his guidance and advice in the cource of this study. He always encouraged me to overcome the difficulties encountered.

Dr. H. Fujimoto advised me about the setting of transponders and gave useful suggestions on the sea experiment. Dr. C. Yang encouraged and helped me much in the experiments. I would like to express my heartful gratitude to them.

I also would like to express sincere thanks to Captain, Emeritus Professor K. Inoue, Emeritus Professor Dr. Y. Miyazaki, Emeritus Professor S. Yanagawa, Professor Dr. E. Hamada and Professor Dr. K. Sato for their encouragements and supports.

Fruitful suggestions were given through discussions with Professor Dr. K. Taira and staff of Submarine Geophysics division of Ocean Research Institute, University of Tokyo.

The crew of research and training vessel Seiyo-Maru, Tokyo University of Fisheries, offered me with hospitality and sincere help during the sea experiment.

The computations were mainly performed at the Information Processing Center, Tokyo University of Fisheries.

Table of Contents

Figure Captions

Chapter 1

Figure 1-1 The relative location between a sound source(S) and the receivers(R_i). T_i and θ_i show, respectively, the propagation time and the transmission angle from the source for i -th sound ray.

Figure 1-2(a) The sound ray diagrams transmitted from a source at the bottom(upper) and at the sea surface(lower) in case of 100 m depth for a given sound speed profile model(left).

Figure 1-2(b) The sound ray diagrams transmitted from a source at the bottom(upper) and at the sea surface(lower) in case of 1 km depth for a given sound speed profile model(left).

Figure 1-2(c) The sound ray diagrams transmitted from a source at the bottom(upper) and at the sea surface(lower) in case of 10 km depth for a given sound speed profile model(left).

Figure 1-3(a), 1-3(b) The left shows the sound speed profiles within 1500m depth in February(a) and May(b) in the Sagami Bay. The right shows the sound ray diagram correspoding to the left profile. A sound source is set at a point by 100m above the sea floor. In the figure, the upward propagation ray (initial transmission angle from the sound source is from 70deg. to 85deg. with the interval 1 deg.) and the downward propagation ray (from 91deg. to 95deg. with the interval 1 degree) are shown.

Figure 1-3(c), 1-3(d) The left shows the sound speed profiles within 1500m depth in August(c) and November(d) in the Sagami Bay. The right shows the sound ray diagram correspoding to the left profile. A sound source is set at a point by 100m above the sea floor. In the figure, the upward propagation ray (initial transmission angle from the sound source is from 70deg. to 85deg. with the interval 1 degree) and the downward propagation ray (from 91deg. to 95deg. with the interval 1 degree) are shown.

Figure 1-4 Left figure shows the models of vertical sound speed profile as a function of depth in February and August in the Sagami Bay. Right figure shows the sound ray diagram based on the left figure. The cases of total reflection at the sea surface are drawn.

Figure 1-5 An observed sound speed profile(solid line) derived from the temperature profile(left) and curve fitted sound speed profile(broken line, right) by the Chebychev function of 3rd degree for the vertical sea temperature profile model for 1km depth.

Figure 1-6(a) Right figure shows the standard deviation(SD) of sound speed error vs. the degree of Chebychev polynomial used for the curve fitting sound speed profile in case of 100 m depth. Left figure shows the sound speed profiles with depth used for the curve fitting. The calculation were made for each season separatedly as indicated by **F** through **D**.
F: February, **A**: April, **J**: June, **AU**: August, **O**: October, **D**: December

Figure 1-6(b) Right figure shows the standard deviation(SD) of sound speed error vs. the degree of Chebychev polynomial used for the curve fitting sound speed profile in case of 1km depth. Left figure shows the sound speed profiles with depth used for the curve fitting. The calculation were made for each season separatedly as indicated by **F** through **D**.
F: February, **A**: April, **J**: June, **AU**: August, **O**: October, **D**: December

Figure 1-6(c) Right figure shows the standard deviation(SD) of sound speed error vs. the degree of Chebychev polynomial used for the curve fitting sound speed profile in case of 10 km depth. Left

Chapter 3

List of Tables

List of Photograph

Introduction

The first idea of ocean acoustic tomography is an observation method by which the variability of oceanic structure in a mesoscale is measured three dimensionally. Since the underwater sound speed depends on sea temperature, salinity and the pressure in the propagation medium, the propagation time of sound wave which involves the integrated information of these parameters is measured precisely in the tomography. Using this characteristics of propagation time the oceanic physical parameters can be estimated by the inversion method.

The history of ocean acoustic tomography is not long. The necessity of global oceanic observation was advocated in the 1970's. The use of sound wave for the observation was grappled first by Munk(1974). Description of oceanic features from the propagation data of acoustic signals requires a method of the inverse technique. Wunsch(1977, and 1978) derived the circulation in the North Atlantic Ocean from hydrographic data by using the inverse method. The ocean acoustic tomography to observe the sea over 1000km square was proposed by Munk and Wunsch in 1979. Then, the sound source with the frequency of 220Hz for tomographic research was developed by Spindel(1979). The preliminary experiments of sound wave propagation were made by Spiesberger et al(1980) and Spindel and Spiesberger(1981) in the Atlantic Ocean, and they succeeded in the separation of multi path signal. A verification experiment of

tomography was made at the MODE area (300km x 300km) in the North Atlantic Ocean and the sound speed anomaly map was reported as the result of the experiment (Ocean Tomography Group, 1982; Cornuelle et al, 1985). Recently, the sound sources network on a global scale for verification of the Earth warming by the ocean acoustic tomography is planned (Munk and Forbes, 1989).

On the other hand, there is also a growing tendency of research by the ocean acoustic tomography in Japan. The Marine Acoustic Society(1986) investigated the present status of the tomography and reviewed the theoretical and the technical problems. Japan Hydrographic Association(1989) carried out the sound transmission test using the M sequence signal at the Sagami Bay and acquired techniques on data processing. The Japan Marine Science and Technology Center is promoting the development of the system of tomography expected to be in operation from 1993 to 1995 to observe the 1000km x 1000km area in real time. Although there are some other activity plans of the research groups of tomography, they are still on planning stages and have not attained any practical applications.

The sound radiated horizontally proceeds in water while being refracted and reflected between the sea surface and the floor according to Snell's law. In the tomography, it is generally required to consider the relative locations of the sound source and the receiver so as to realize the selection of effective paths of sound and to get as much information of oceanic parameters as possible. The microtomographic technique proposed in this paper gives an estimation method of the vertical sound speed profile, which is expressed in terms of a high degree Chebychev polynomial in a scale from several hundreds meters to 10 kilometers. In the microtomographic approach, the round-trip propagation time of acoustic signal propagated directly between a

sound source fixed on the sea floor and a receiver at the sea surface is used. As it is assumed in this study that the sea water has a layered structure, i.e., the vertical structure of sound speed is uniform horizontally within the target area, the sound speed structure thus derived shows a mean structure in the area.

If the micro tomographic technique proposed here is achieved by overcoming many technical problems, it is useful as a new tool of acoustic remote sensing technique for monitoring environmental change in the coastal fishing ground or oceanic physical structures at a specific area.

Chapter 1 deals with the concept of microtomography and the theoretical background. The function to analytically express the sound speed profile is derived from the inversion method. The areal limit in which the microtomography is applicable is also discussed by using the sound ray theory. The algorithm for positioning sound source(transponder) fixed at the sea floor is described because it is important to aid the microtomographic technique, though positioning itself is not related directly to the tomography. The positioning is made by use of slant range measured acoustically. The results of preliminary experiments of the microtomograpy in the Sagami Bay made in 1991 and the verification experiment in 1992 are mentioned in Chapter 2. The method of experiment and the performance of instruments are explained and the estimation accuracy of sound speed profile is evaluated. In Chapter 3 the method to improve the estimation accuracy of temperature in shallow sea is discussed through the simulation study. A model of total system for the microtomography is proposed by taking the results described in the previous chapters into consideration. Summary of the results from this study and the problems or tasks of proposed system are discussed in Chapter 4 as the conclusion.

Chapter 1

1. Theoretical Background of Micro Tomography

1.1 Concept

Figure 1-1 shows a fundamental arrangement for the microtomography in which a sound source S is fixed at the sea floor and the receivers R_i , i =1, 2,... , n at the sea surface. In this case, a sound signal transmitted with an initial angle θ_i from the source reaches directly the receivers R_i while being refracted according to the Snell's law. In microtomography, a propagation time T_i of the sound signal propagating directly is used; the signal reflected from the bottom or the surface is not used because it is unstable and weak due to the scattering or the absorption phenomena. The characteristics of microtomography are: (1)The sound signal propagating in the vertical direction between the sea surface and the sea floor is used positively, whereas the long range tomography uses the sound signal propagating between the sound sources and the receivers located almost horizontally. (2)It does not need a giant instrument because the propagation distance of sound signal is short. (3)A stable and higher ratio of S/N is expected as the direct propagation wave is handled only. (4)Variability of mean vertical profiles of sound speed and sea temperature can be monitored by a long term and continuous observation.

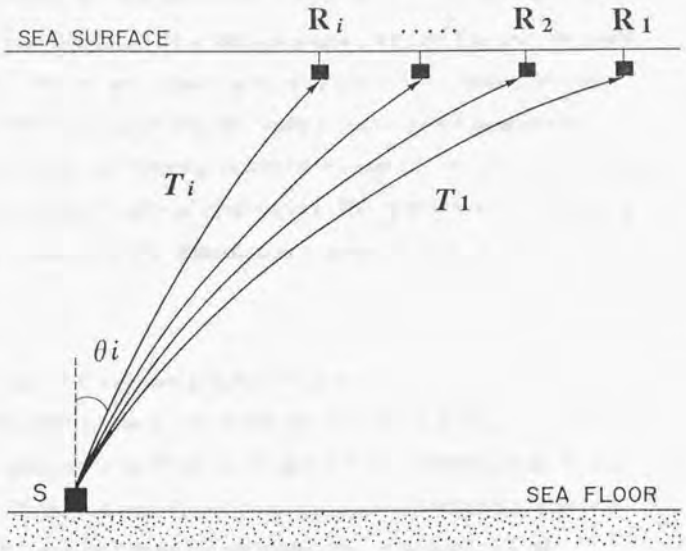

Figure 1-1 The relative location between a sound source(S) and the receivers(R_i). T_i and θ_i show respectively the travel time and the transmission angle from the source for i th sound ray.

The concept of processing procedure is as follows: The estimation of sound speed structure is made by constructing the observation equations that contain the measured propagation time and the calculated propagation time derived from the sound speed function expressed by the Chebychev polynomial. Then, the coefficients of the best-fit polynomial to the observed sound speed profile are computed from the observation equations by inversion. It is assumed, in this tomographic technique, that the vertical sound speed is uniform horizontally and is constant with time because of the small scale of the area and the short term of observation. The approximation method by the polynomial and the algorithm of inversion will be explained later in detail.

The Range of Microtomography Available

In order to know the limitation of horizontal range to which microtomography method can be applied, the distribution of the ray path of the signal transmitted from a source is considered. Figure 1-2(a), 2(b) and 2(c) show the path diagrams of acoustic signal transmitted from a source at the bottom to the sea surface(upper) and a source at the sea surface to the bottom(lower). As the round-trip propagation of the sound signal between the bottom and the surface may be used for the sake of cancelling the influence of water current along the sound ray path, upward and downward transmissions are both drawn in the figures. Three cases with depths, i.e., 100 m(Figure 1-2(a)), 1 km(1-2(b)) and 10 km(1-2(c)) are illustrated for given sound speed profiles. Although the existence of 10 km depth is very rare in the actual ocean, the depth was selected so as to give the upper limit of the range for microtomography using the ray of direct propagation. The sound speed profiles are those derived from typical

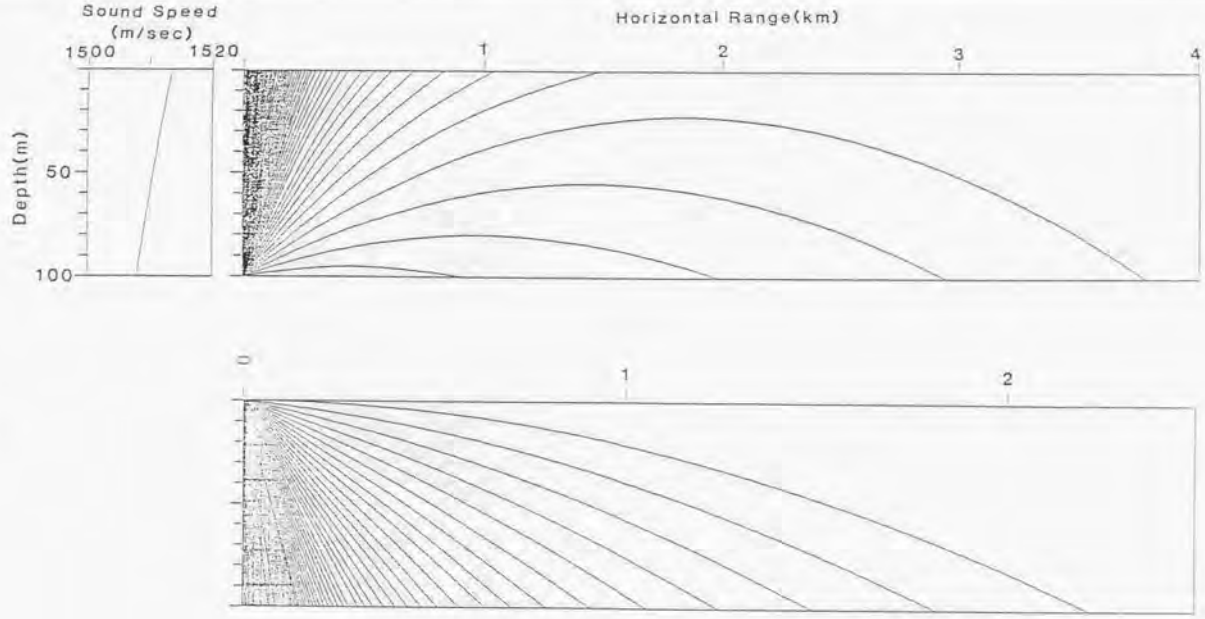

Figure 1-2(a) The sound ray diagrams transmitted from a source at the bottom(upper) and at the sea surface(lower) in case of 100 meter depth for a given sound speed profile model(left).

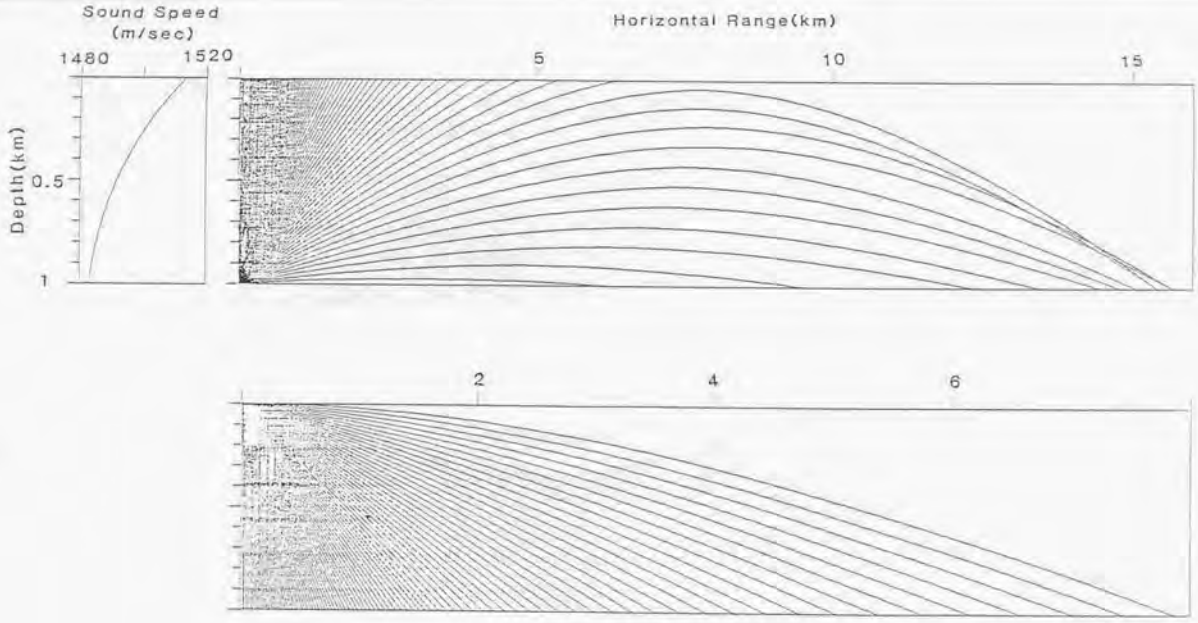

Figure 1-2(b) The sound ray diagrams transmitted from a source at the bottom(upper) and at the sea surface(lower) in case of 1 km depth for a given sound speed profile model(left).

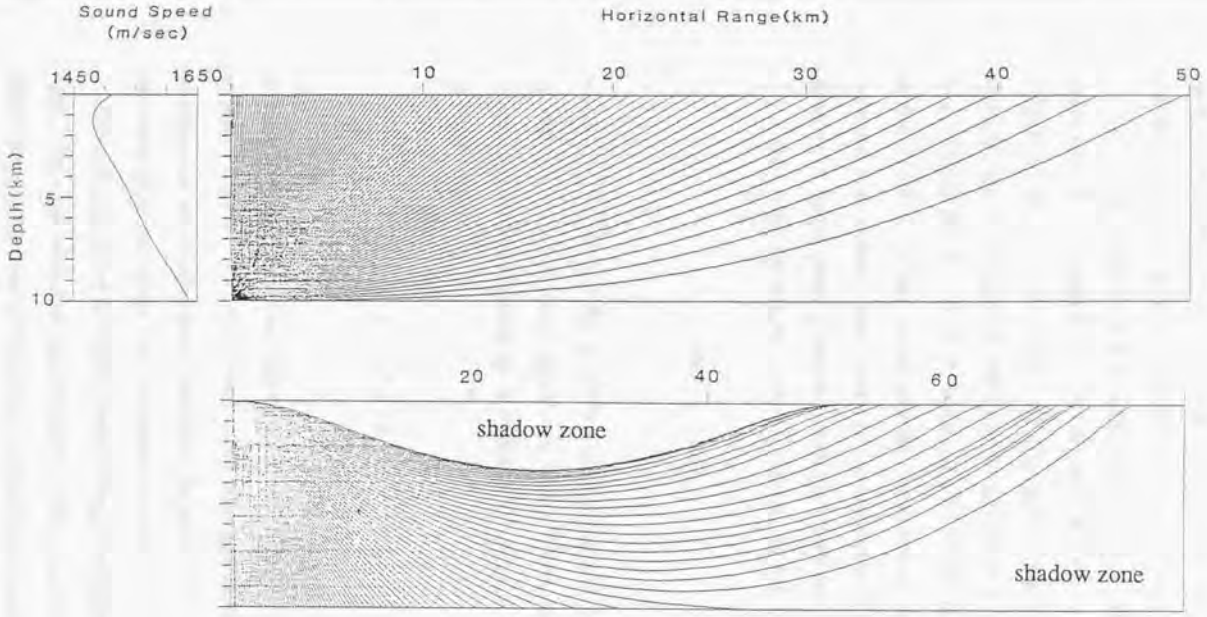

Figure 1-2(c) The sound ray diagrams transmitted from a source at the bottom(upper) and at the sea surface(lower) in case of 10 km depth for a given sound speed profile model(left).

temperature distribution at the Sagami Bay which is used as a model at middle latitude of the western Pacific Ocean in early summer.

The transmitted angle θ_i (see Figure 1-1) of the ray is changed every one degree from zero to 90 degrees in each figure. The total reflection phenomena occur in ray diagrams of the upward transmission in the case of 100 m and 1 km depth and, the downward transmission in the case of 10 km depth. When the angle of the ray path exceeds the critical angle during transmission, the ray is bent downward or upward and returns to the sea floor or the sea surface. Suppose a sound propagation at a boundary surface of different media. Then, the sound propagates according to the Snell's law given by

$$\sin \theta_f = \frac{V_f}{V_s} \sin \theta_s \quad , \tag{1-1}$$

where, V_s and θ_s are the incident sound speed and angle, and V_f and θ_f are the refracted sound speed and angle. When the total reflection occurs, the refracted angle θ_f is equal to 90 degrees. Then, equation (1-1) becomes

$$1 = \frac{V_f}{V_s} \sin \theta_s \quad . \tag{1-2}$$

In oder to satisfy the condition of equation (1-2), V_f must be equal to or larger than V_s i.e., the sound speed structure must have positive gradient for the propagating direction. In general, the vertical structure of sound speed has the minimum point of speed at about 500 ~1000 m depth called SOFAR(Sound Fixing and Ranging) channel zone. The total reflection occurs easily in the layer shallower than the SOFAR channel zone in the case of upward transmission and in the

layer deeper than the zone in the case of downward transmission, though the occurrence of total reflection is related to the initial transmission angle of the signal from the sound source. This is the reason why the phenomena of the total reflection is seen for the upward propagation in the case of 100 m and 1 km depth and, the downward propagation in the case of 10 km depth.

The area where the microtomographic approach is possible is limited by the total reflection. The limitation radius of the circle at the sea surface is about 2 km (θ_i =85.4 degree), 8 km (θ_i =78.6 degree) and 50 km (θ_i =68.5 degree) for the depths of 100 m, 1 km and 10 km, respectively. The sound speed varies with time and place, but the limitation will not differ largely from the value above mentioned.

In order to know the effect of the seasonal change of water temperature on the sound ray, the Sagami Bay located at the southern coast of Japan is selected as a model area to give a more definite image to the microtomographic approach. A part of this is reported by Kakihara and Segawa(1992). The sound source is assumed to be installed at a depth of 1500m in the Sagami Trough which runs in the middle of the Sagami Bay down to the Japan Trench.

The left profiles in Figures 1-3(a), (b), (c) and (d) show typical sound speed (calculated from the sea temperature data provided from Japan Oceanographic Data Center(JODC), sea area code 49C, personal communication) within 1500m depth in February(a), May(b), August(c) and November(d) in the Sagami Bay. The code 49C area which is surrounded by 1 degree square in latitude 34 deg.N ~ 35 deg.N and in longitude139 deg.E ~ 140 deg.E, is located at the southern Sagami Bay and covers the target area. The right profiles in Figures 1-3(a), (b), (c) and (d) show the sound ray diagram corresponding to the sound speed profile(left). The sound ray diagrams

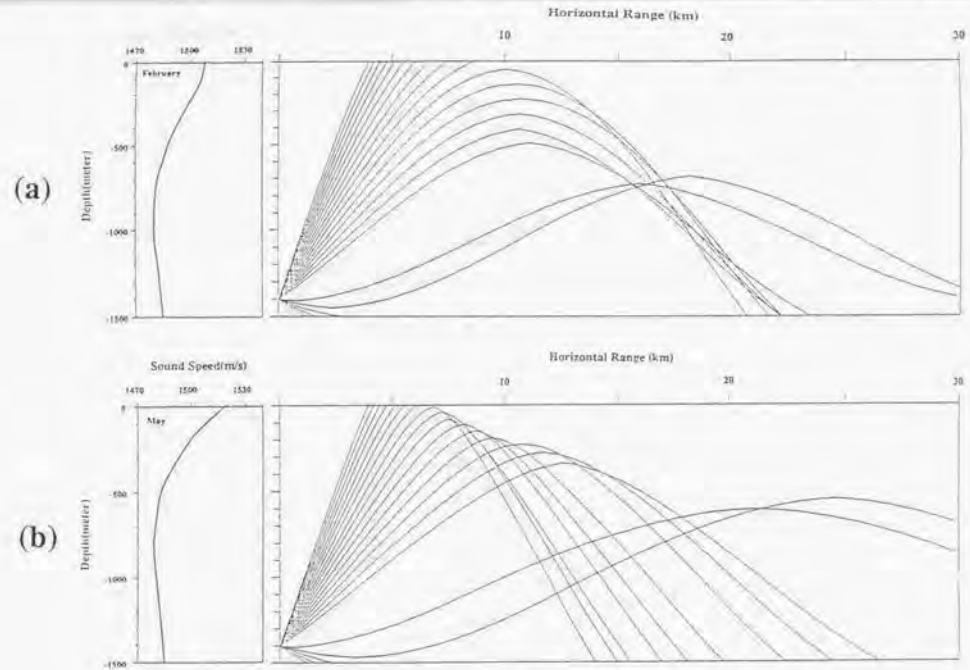

Figure 1-3(a), 1-3(b) The left shows the sound speed profiles within 1500m depth in February(a) and May(b) in the Sagami Bay. The right shows the sound ray diagram correspoding to the left profile. A sound source is set at a point by 100m above the sea floor. In the figure, the upward propagation ray (initial transmission angle from the sound source is from 70deg. to 85deg. with the interval 1 deg.) and the downward propagation ray (from 91deg. to 95deg. with the interval 1 degree) are shown.

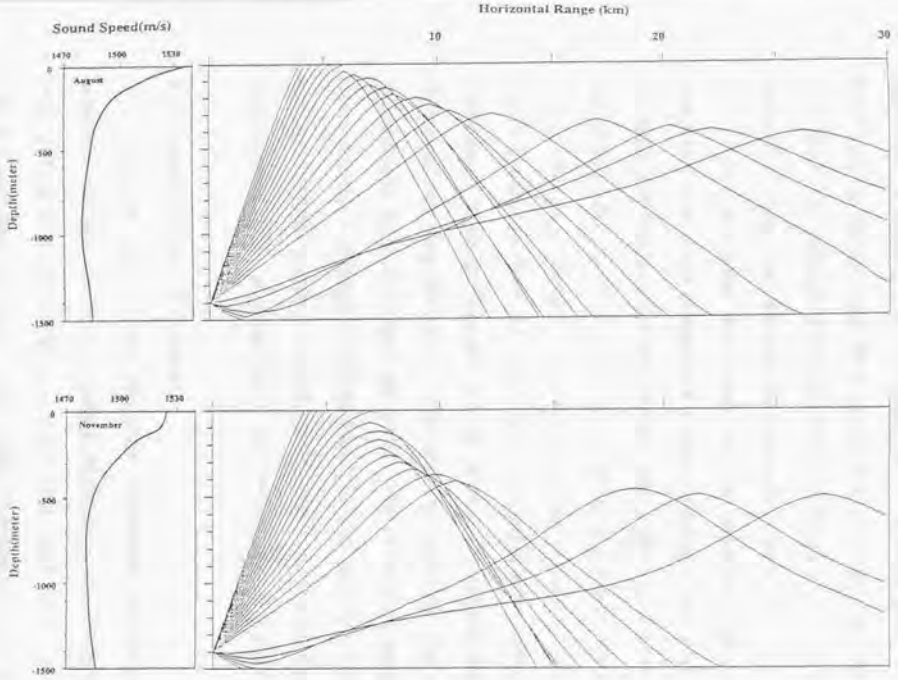

(c)

(d)

Figure 1-3(c), 1-3(d) The left shows the sound speed profiles within 1500m depth in August(c) and November(d) in the Sagami Bay. The right shows the sound ray diagram correspoding to the left profile. A sound source is set at a point by 100m above the sea floor. In the figure, the upward propagation ray (initial transmission angle from the sound source is from 70deg. to 85deg. with the interval 1 degree) and the downward propagation ray (from 91deg. to 95deg. with the interval 1 degree) are shown.

in the right show the case when the sound source is installed by 100m above the sea floor. This happens in the actual experiment because the sea floor is not necessarily flat. The sound ray diagrams in the figures show the ray paths for selected initial transmission angles with the interval of 1 degree. The rays transmitted upward have the initial transmission angles from 70 degrees to 85 degrees from the vertical and those transmitted downward from 91 degrees to 95 degrees. The paths after reflection are not shown in the figures.

It is found from the figures that the maximum range in which a direct acoustic wave is received at the surface is about 7km in spring(May) and autumn(November), about 6km in summer(August) and about 12km in winter(February). No direct sound waves transmitted downward initially reach the sea surface all the year round. Figure1-4 shows the models of vertical sound speed profile as a function of depth in February and August in the Sagami Bay(left) and the sound ray diagram based on the left figure(right). The cases of total reflection at the sea surface are drawn. The maximum range in winter becomes twice as large comparing with that in summer. This is because the sound speed gradient with depth is smaller in winter than in summer due to the appearance of the surface mixed layer in winter.

1.2 Sound Speed Function

When the sound speed structure is estimated by the inversion method, both the observed propagation time and the calculated propagation time are needed as above mentioned. In this section the sound speed function used to derive the propagation time is described.

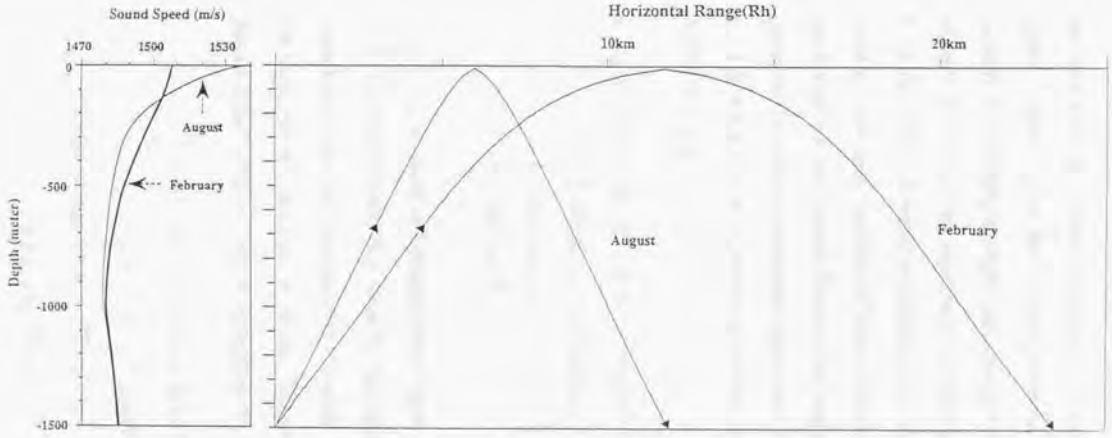

Figure 1-4 Left figure shows the models of vertical sound speed profile as a function of depth in February and August in the Sagami Bay. Right figure shows the sound ray diagram based on the left figure. The cases of total refraction at the sea surface are drawn.

Mackenzie's Equation

An 'observed' propagation time is determined by the sound speed derived from the observed oceanic parameters. The underwater sound speed depends upon the oceanic physical variables, i.e., temperature, salinity and depth(pressure) and is expressed by a function if the effect of bubbles or oceanic organisms is neglected. Leroy(1969) and Medwin(1975) showed an empirical equation of sound speed with a simple form as a function of three variables. Mackenzie(1981) published a sound speed function having nine terms which is simple and practical for digital computer operation. This equation is commonly used in the acoustic engineering and the acoustic oceanography. His formulation is

$$\begin{aligned} V_o(t, s, z) = {} & 1448.96 + 4.591t - 5.304\times10^{-2}t^2 \\ & + 2.374\times10^{-4}t^3 + 1.340(s - 35) \\ & + 1.630\times10^{-2}z + 1.675\times10^{-7}z^2 - 1.025\times10^{-2}t(s - 35) \\ & - 7.139\times10^{-13}t z^3, \end{aligned} \tag{1-3}$$

where V_o is observed sound speed (m/sec), and t, s and z correspond to a sea temperature(°C), salinity(‰) and depth(m), respectively. This equation is believed to keep a 0.15 m/sec accuracy in standard deviation for even the sea of extreme depth. The partial derivative expressions of sound speed with respect to temperature, depth and salinity are

$$\begin{aligned} \frac{\partial V_o}{\partial t} = {} & 4.591 - 0.1061t + 0.00071t^2 \\ & - 7.139\times10^{-13}z^3 - 0.01025(s - 35), \end{aligned} \tag{1-4}$$

$$\begin{aligned} \frac{\partial V_o}{\partial z} = {} & 0.0163 + 3.350\times10^{-7}z \\ & - 2.142\times10^{-12}t z^2 \end{aligned} \tag{1-5}$$

and $$\frac{\partial V_o}{\partial s} = 1.340 - 0.01025t \quad . \qquad (1\text{-}6)$$

When the depth is 0 m and the temperature is 0 °C, $\partial V_0/\partial t$ becomes the maximum of 4.59 m/sec per 1 °C. The contribution of temperature variation to the sound speed is the largest compared with other parameters in the shallow layer where the temperature varies steeply.

As the variation of temperature is very small at the deeper depth, the sound speed vaires by about 0.016m/sec per 1m depth shown in equation(1-5). The SOFAR channel where the sound speed becomes minimum is formed due to both the decrease of temperature in the main thermocline at the shallow layer and the pressure dependency on sound speed at deeper depth.

When the salinity increases by 1 ‰ from 35 ‰ at zero °C of temperature, the sound speed increases by 1.34 m/sec as shown in equation(1-6). Since the departure from 35 ‰ is generally less than 1 ‰ and the sea temperature is higher than zero °C, the contribution of salinity to sound speed is very small in the study sea area.

Modeling of Sound Speed Function

The 'calculated' propagation time is obtained from the sound speed function approximated to the actual sound speed structure.The sound speed function is expressed by a continuous function with the depth as a parameter. As for the expression of vertical sound speed profile, Okujima et al(1985) attempted to use an exponential function in the Kuroshio current area and reported to have obtained a good result. Kakihara and Segawa(1991) tried to employ the expression by a polynomial. However, since the instability of solution in the inversion process was seen for the high degree polynomial, it was replaced by a Chebychev polynomial for modeling of the sound speed profile, which

is stable at high degrees and its precision of approximation is better than the other polynomial. The definition of Chebychev's polynomial is

$$T_n(x) = \cos(n \arccos x)$$
$$-1 \le x \le 1 \quad , (n = 0,1,2,\cdots). \tag{1-7}$$

for which a recurrence formula holds as

$$T_{n+1}(x) - 2xT_n(x) + T_{n-1}(x) = 0 \quad . \tag{1-8}$$

The sound speed function $Vc\ (x)$ proposed here is given by the following linear expression.

$$V_c(x) = \sum_{j=0}^{m} C_j \cdot T_j(x) \quad , \tag{1-9}$$

where Cj is the coefficient of Chebychev polynomial. The depth(z) is transformed to (x), where $-1 \le x \le 1$, i.e.,

$$x = \frac{2z - (a+b)}{b - a} \quad , \tag{1-10}$$

where $a \le z \le b$. Using (1-10), we can calculate the sound speed at any depth. If the best fit function to actual sound speed structure is computed, the coefficients Cj in $Vc\ (z\ )$ function is derived directly by the least squares method.

Figure 1-5 shows an example of the sound speed profiles at 1 km depth model derived from Vo and Vc functions for the temperature speed profile and the dashed line is a curve fitted profile by 3rd degree Chebychev polynomial. In this case, the error of calculated sound speed

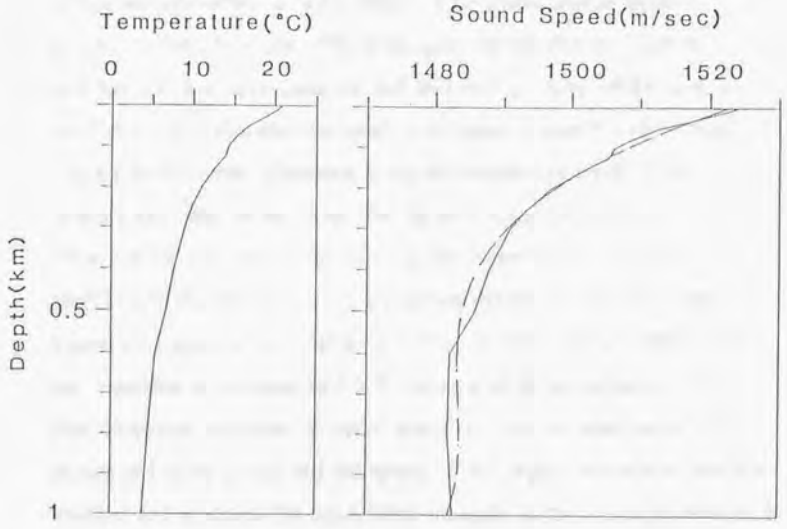

Figure 1-5 An observed sound speed profile(solid line) derived from the temperature profile(left) and curve fitted sound speed profile(broken line, right) by the Chebychev function of 3rd degree for the vertical sea temperature profile model for 1km depth.

compared with the actual sound speed shown by the solid line is 2.03 m/sec maximum and 1.29 m/sec in standard deviation(SD).

The errors of modeled sound speed functions were simulated for the case of various depths, sound speed profiles and degrees of polynomial. Figures 1-6(a), 1-6(b) and 1-6(c) show the standard deviation(SD) errors of curve fitted sound speed profile against degrees of the Chebychev function(right) for given sound speed profiles(left) for three cases of 100 m(1-6(a)), 1 km(1-6(b)) and 10 km(1-6(c)) and SDs are evaluated in relation to months. The sound speed profiles were calculated from the monthly average of sea temperature data offered from the Japan Oceanographic Data Center(JODC) in the southern part of the Sagami Bay. The sound speed profiles and the SD curves are illustrated every two month in the figure. In Figure 1-6(c), the temperature at depth larger than 1.5 km was regarded as constant of 2.5 °C because of the absence of JODC data. Seasonal variation of sound speed are obvious near surface as shown in Figure 1-6(a) and the speed is the largest in August and the smallest in February. No remarkable changes in the speed profiles with months are seen at depth deeper than 150 m(Figure 1-6(b)). As the temperature at depth deeper than 1.5 km is assumed constant, the sound speed increases linearly with the averaged rate of 0.016 m/sec with depth due to the effect of the pressure only as seen from equation(1-5).

The SD of sound speed error decreases rapidly with the degrees of polynomials employed in each figure. This tendency is independent of the observation month as well as the depth of the model. The curve fitting accuracy by the polynomial is the best in February(winter) and is the worst in August(summer) as shown in the figures. The average errors were almost zero in all cases. The SD becomes very small for the degree larger than 7 in 100 m depth model, 0.2 m/sec ~ 0.5 m/sec

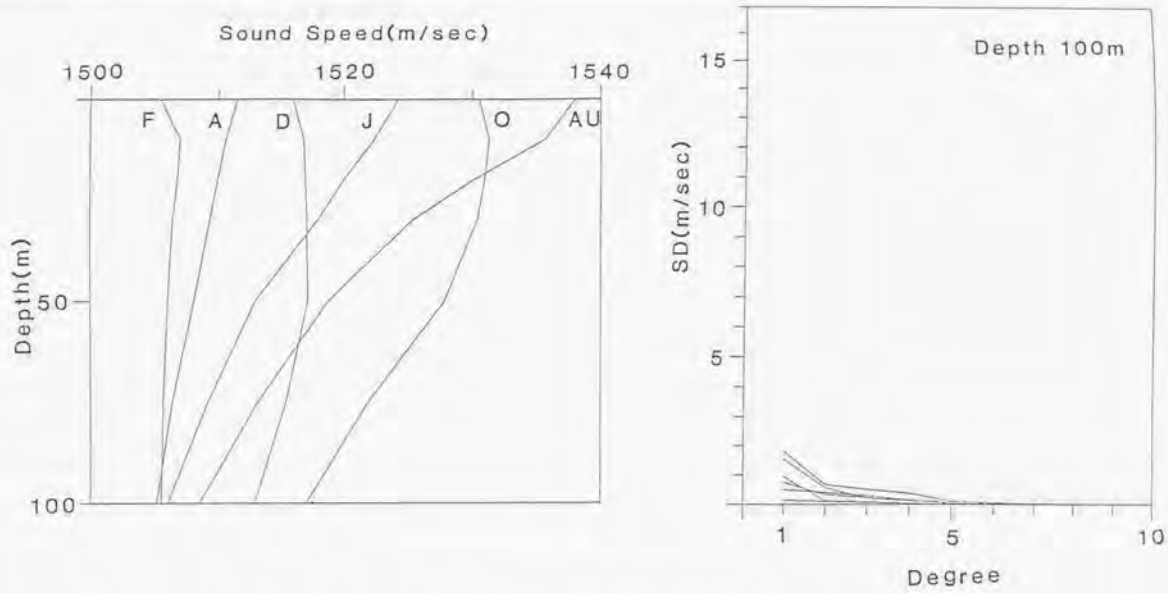

Figure 1-6(a) Right figure shows the standard deviation(SD) of sound speed error vs. the degree of Chebychev polynomial used for the curve fitting sound speed profile in case of 100 m depth. Left figure shows the sound speed profiles with depth used for the curve fitting. The calculation were made for each season separatedly as indicated by **F** through **D**.
F: February, **A**: April, **J**: June, **AU**: August, **O**: October, **D**: December

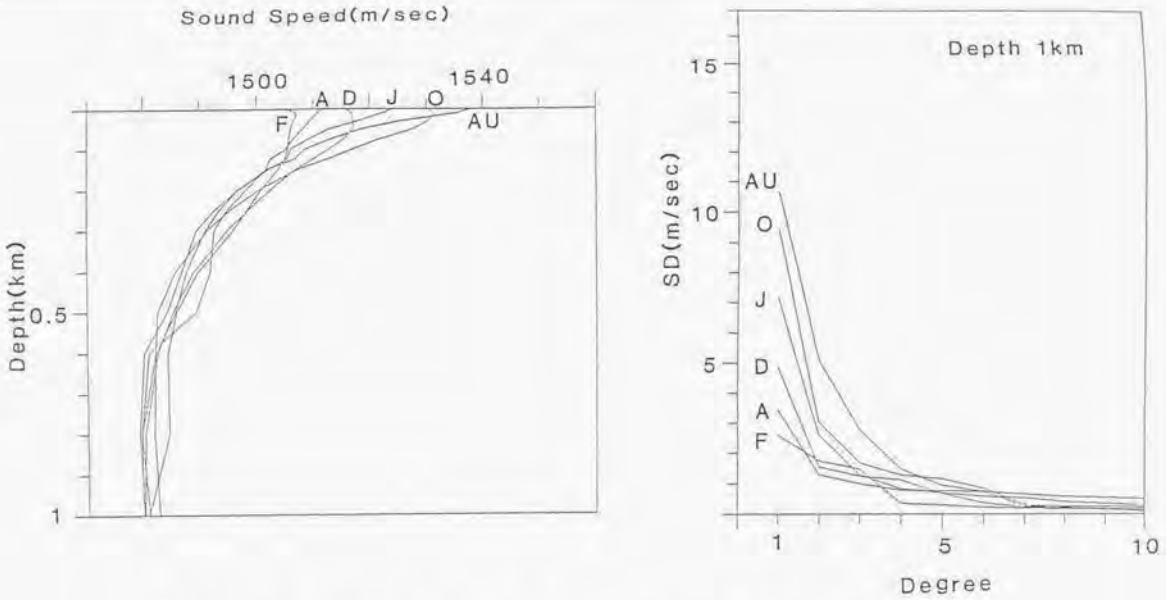

Figure 1-6(b) Right figure shows the standard deviation(SD) of sound speed error vs. the degree of Chebychev polynomial used for the curve fitting sound speed profile in case of1 km depth. Left figure shows the sound speed profiles with depth used for the curve fitting. The calculation were made for each season separatedly as indicated by **F** through **D**.
F: February, **A**: April, **J**: June, **AU**: August, **O**: October, **D**: December

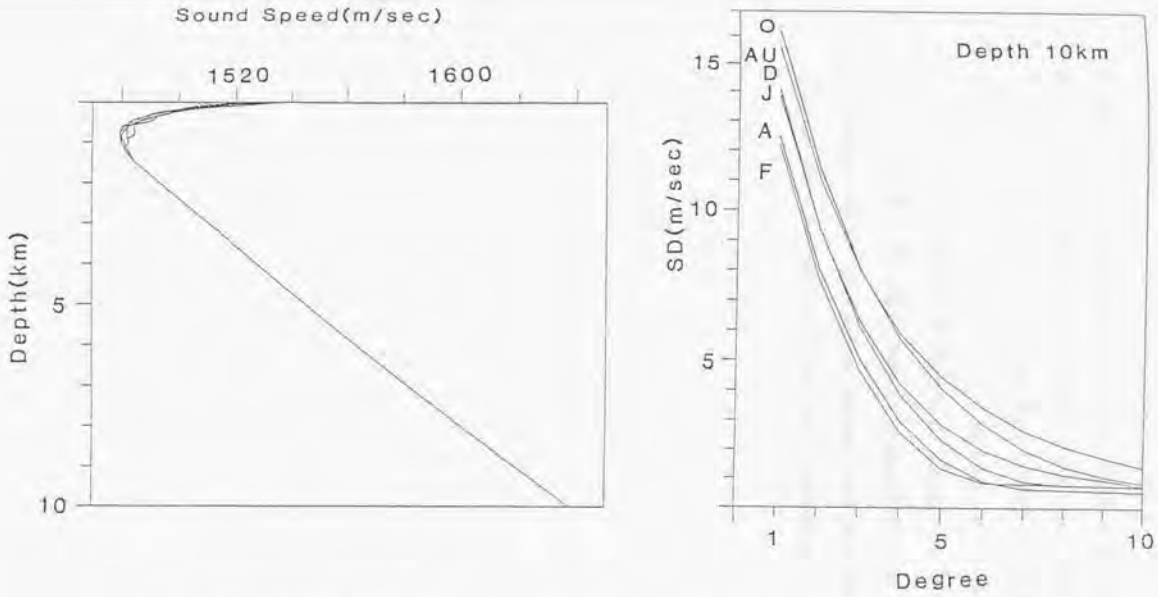

Figure 1-6(c) Right figure shows the standard deviation(SD) of sound speed error vs. the degree of Chebychev polynomial used for the curve fitting sound speed profile in case of 10 km depth. Left figure shows the sound speed profiles with depth used for the curve fitting. The calculation were made for each season separatedly as indicated by **F** through **D**.
F: February, **A**: April, **J**: June, **AU**: August, **O**: October, **D**: December

for the degree larger than 6 in 1 km model and 0.5 m/sec ~ 1.5 m/sec for the degree larger than 8 in 10 km depth model. When the sound speed change rate is assumed 3 m/sec per 1 °C change of the sea temperature, the SDs of temperature converted from speed error above mentioned become 0.07 ~ 0.17 °C in 1 km depth case and 0.17 ~ 0.5 °C in 10 km depth case. If the degree of polynomial is the same, the SDs become larger with the depth of the model. It may be interpreted that SD value shown in this figure indicates the limitation of curve fit using Chebychev polynomial for the vertical sound speed structure.

1.3 Estimation Method of Sound Speed

Figure 1-7 shows the flow chart of processing procedure.

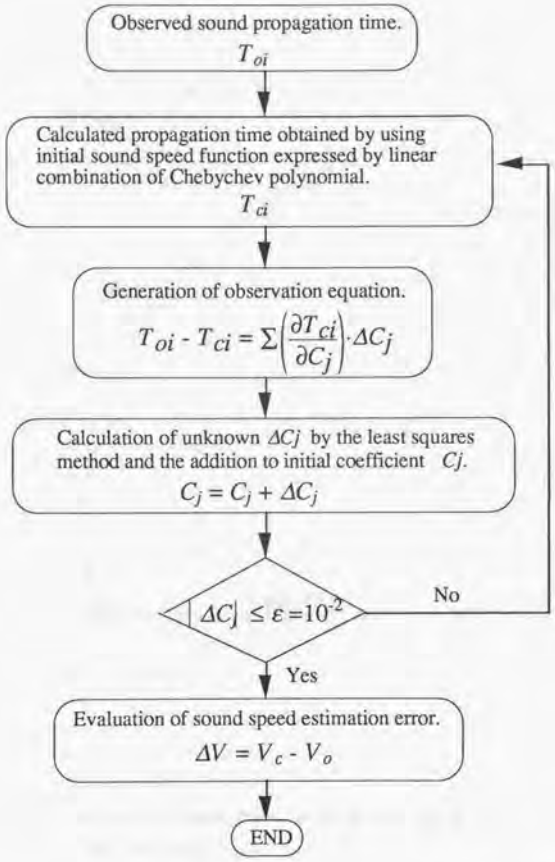

Figure 1-7 The flow chart of processing procedure.

In the first step, a suitable sound speed function expressed by the linear combination of Chebychev polynomials as shown in equation(1-9) is given as an initial sound speed profile to calculate the propagation time

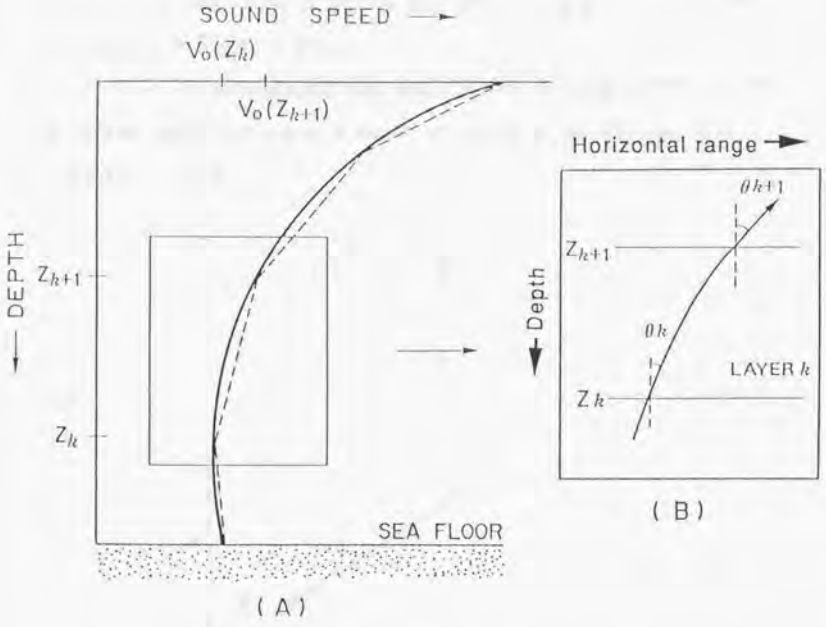

Figure 1-8 Illustration to explain the computation method of propagation time and horizontal range.

(A): The relation between an actual sound speed profile(solid line) and a linearly segmented sound speed profile(broken line).

(B): The sound ray for the linearly segmented sound speed corresponding to the enclosed square of (A).

T_{ci}. Figure 1-8(A) and Figure 1-8(B) illustrate the calculation method of propagation time from a given sound speed profile. The solid line in Figure 1-8(A) is the sound speed profile initially given and the broken line is the approximated sound speed profile using linear segments. Figure 1-8(B) shows the sound ray path inside a segment layer enclosed by a square in Figure 1-8(A).

Now, if a propagation time and a horizontal range within a layer k, whose upper depth is z_{k+1} and lower depth z_k, be ΔT_k and Δr_k, respectively, then

$$\Delta T_k = \int_{z_k}^{z_{k+1}} dt \tag{1-11}$$

and

$$\Delta r_k = \int_{z_k}^{z_{k+1}} dr \tag{1-12}$$

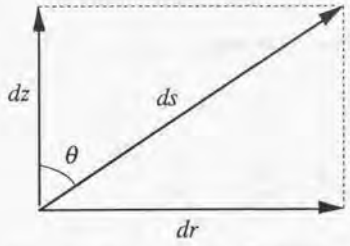

Figure 1-9 Sound ray path difference ds v.s. horizontal and vertical displacement dr and dz.

The sound ray path difference ds and the propagation time of the sound dt are

$$ds = \frac{dz}{\cos\theta} \tag{1-13}$$

$$dt = \frac{ds}{V_c(z)} = \frac{dz}{V_c(z)\cos\theta},$$

and (1-14)

where dz is the vertical displacement, and the horizontal displacement is

$$dr = \tan\theta\, dz. \tag{1-15}$$

For more convenient expressions, the Snell's law is used to replace $\sin\theta$, $\cos\theta$ and $\tan\theta$ as the following:

$$\sin\theta = aV_c(z), \tag{1-16}$$

$$\cos\theta = \left[1 - a^2V_c^2(z)\right]^{1/2}, \tag{1-17}$$

and

$$\tan\theta = aV_c(z)\left[1 - a^2V_c^2(z)\right]^{-1/2}. \tag{1-18}$$

where 'a ' is Snell's constant(see, Eq.1-29).
Then, equation (1-11) and (1-12) are expressed as

$$\Delta T_k = \int_{z_k}^{z_{k+1}} \frac{dz}{V_c(z)\left[1 - a^2V_c^2(z)\right]^{1/2}} \tag{1-19}$$

and

$$\Delta r_k = \int_{z_k}^{z_{k+1}} \frac{aV_c(z)dz}{\left[1 - a^2V_c^2(z)\right]^{1/2}}. \tag{1-20}$$

When the gradient b_k of the sound speed between depth z_k and z_{k+1} is regarded almost constant, it is expressed as

$$b_k = \frac{V_c(z_k) - V_c(z_{k+1})}{z_k - z_{k+1}}. \tag{1-21}$$

Then the integrals (1-19) and (1-20) are performed as follows:
Equation (1-19) is rewritten as

$$\Delta T_k = \frac{1}{b_k} \int_{V_c(z_k)}^{V_c(z_{k+1})} \frac{dV_c(z)}{V_c(z)\left[1 - a^2 V_c^2(z)\right]^{1/2}} \qquad (1\text{-}22)$$

using equation (1-21). When equation (1-16) and (1-17) are put into (1-22), then we get

$$\begin{aligned} \Delta T_k &= \frac{1}{b_k} \int_{\theta_k}^{\theta_{k+1}} \frac{\frac{1}{a}\cos\theta \, d\theta}{\frac{1}{a}\cos\theta \, \sin\theta} \\ &= \frac{1}{b_k} \int_{\theta_k}^{\theta_{k+1}} \frac{d\theta}{\sin\theta} \\ &= \frac{1}{b_k} \left[\ln \tan \frac{\theta}{2} \right]_{\theta_k}^{\theta_{k+1}} . \end{aligned} \qquad (1\text{-}23)$$

On the other hand, it is evident that

$$\tan \frac{\theta}{2} = \frac{1 - \cos\theta}{\sin\theta} \qquad \text{for } 0 < \theta < 90^\circ . \qquad (1\text{-}24)$$

From (1-23) and (1-24), we get

$$\Delta T_k = \frac{1}{b_k} \ln \left[\frac{\sin\theta_k (1 - \cos\theta_{k+1})}{\sin\theta_{k+1} (1 - \cos\theta_k)} \right] . \qquad (1\text{-}25)$$

If equation (1-16) is again put to (1-25), then we have

$$\Delta T_k = \frac{1}{b_k} \ln\left[\frac{V_c(z_k)(1 - \cos\theta_{k+1})}{V_c(z_{k+1})(1 - \cos\theta_k)}\right]. \qquad (1\text{-}26)$$

Equation (1-20) is rewritten similarly as

$$\Delta r_k = \frac{1}{b_k}\int_{V_c(z_k)}^{V_c(z_{k+1})} \frac{aV_c(z)dV_c(z)}{V_c(z)\left[1 - a^2V_c^2(z)\right]^{1/2}}$$
$$= \frac{1}{ab_k}\left\{\left[1 - a^2V_c^2(z_k)\right]^{1/2} - \left[1 - a^2V_c^2(z_{k+1})\right]^{1/2}\right\}. \qquad (1\text{-}27)$$

Put equation (1-17), then (1-27) becomes

$$\Delta r_k = \frac{1}{a\ b_k}(\cos\theta_k - \cos\theta_{k+1}). \qquad (1\text{-}28)$$

These formulations are after Clay(1977).

The θ_k and θ_{k+1} indicate the angles of incident at the depth of z_k and z_{k+1}. The relation of θ_k and θ_{k+1} is expressed by the Snell's law.

$$\frac{\sin\theta_k}{V_c(z_k)} = \frac{\sin\theta_{k+1}}{V_c(z_{k+1})} = a. \qquad (1\text{-}29)$$

'a' is called Snell's constant, and this means that a sound wave propagates keeping the value of 'a' in the medium which has different physical characteristics. The propagation time and the horizontal range of the sound wave between a sound source at the bottom and a receiver at the sea surface are expressed finally by the sum of propagation time and horizontal range of each linear segment, as

$$T_{ci} = \sum_{k=1}^{l} \Delta T_k \qquad (1\text{-}30)$$

$$r_{ci} = \sum_{k=1}^{i} \Delta r_k$$

and (1-31)

The subscript i of T_c corresponds to a sound ray transmitted with a different initial angle 'i' at the sound source.

When the observed propagation time is denoted by T_{oi}, the following observation equation holds:

$$T_{oi} - T_{ci} = \sum_{j=0}^{m} \frac{\partial T_{ci}}{\partial C_j} \cdot \Delta C_j \quad , \tag{1-32}$$

Suppose the propagation time T_{ci} is a function of coefficient C_j of Chebychev polynomial, i.e., $T_{ci} = T_{ci}(C_0, \cdots, C_j, \cdots, C_m)$. Then the partial derivative in equation(1-32) is computed by

$$\frac{\partial T_{ci}}{\partial C_j} = \frac{T_{ci}(C_0, \cdots, C_j + \delta C_j, \cdots, C_m) - T_{ci}(C_0, \cdots, C_j, \cdots, C_m)}{\delta C_j} \quad . \tag{1-33}$$

Solving this observation equation leads to a linear inversion solution to calculate the coefficient Cj's of the polynomials to approximate the vertical sound speed structure. In order to solve the observation equation, the number of propagation data must be more than m+1. The unknowns ΔC_j calculated by the least squares method is added to the initial C_j, which is made repeatedly until it reaches a threshold value.

$$C_j = C_j + \Delta C_j \quad . \tag{1-34}$$

The difference between calculated $V_c(z)$ with the final C_j and the observed $V_o(z)$ is the estimation error $\Delta V(z)$ of the sound speed at depth z.

1.4 Sound Source Positioning

The relative position of the sound source and the receiver is very important for the micro tomographic method and the inaccuracy of the position of the sound source has a large influence on the estimation accuracy of the sound speed structure.

In this section is described the algorithm of positioning of the sound source by use of the least squares method using the data of slant range between the sound source to be located and the receiver whose position is known correctly. Kakihara and Segawa(1991) reported the positioning algorithm and the accuracy of the sound source. When the sound propagates through different media, its behaviour is determined by the physical parameters. The sound ray in water is refracted according to the Snell's law. In the calculation of the position of an underwater body, the sound speed is commonly treated as a constant and the sound ray path is supposed to be straight.

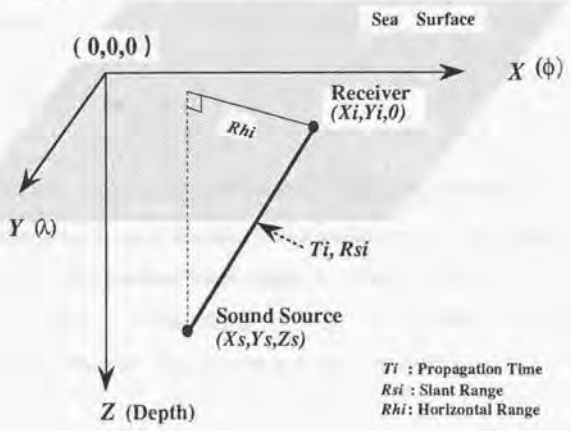

Figure 1-10 The relationship between the sound source position(Xs, Ys, Zs) and the receiver position(Xi , Yi , Zi) in three dimensional coordinate.

Figure 1-10 shows the relationship between positions of a sound source (X_S , Y_S , Z_S) and a receiver (X_i , Y_i , 0). The subscript i corresponds to i-th sound ray propagated directly from the sound source to the receiver. The X -Y axes are taken on the sea surface and Z is taken positive downwards with zero at surface. The receiver is supposed to be on the sea surface. If X and Y coordinates are converted to the world geodetic coordinate system, X and Y axes can be treated as latitude (ϕ) and longitude (λ), respectively. In this section, however, a relative coordinate system whose origin is set arbitrarily on the sea suface is used and the conversion between coordinate systems is not made.

Calculation of the positioning of sound source is carried out according to the following procedure. An estimated position (X'_S , Y'_S , Z'_S) of the sound source is first given as an initial value, because the correct position is unknown. The 'calculated' slant range R_{sci} is expressed by

$$R_{sci} = \sqrt{(X_i - X'_s)^2 + (Y_i - Y'_s)^2 + Z'^2_s}, \qquad (1\text{-}35)$$

where X_i and Y_i coordinates on the sea surface are observed by a precise positioning system like the micro wave positioning system. On the other hand, the 'correct' slant range R_{si} derived from the propagation time T_i and the correct average sound speed $\overline{V_i}$, which is calculated from observed sound speed profile, is written as

$$R_{si} = \overline{V_i} \cdot T_i , \qquad (1\text{-}36)$$

The difference of R_{si} and R_{sci} is caused by the difference in position (ΔX, ΔY, ΔZ) between the initial and correct positions of the sound source. Therefore the following observation equation is generated.

$$R_{si} - R_{sci} = \frac{\partial R_{sci}}{\partial X}\Delta X + \frac{\partial R_{sci}}{\partial Y}\Delta Y + \frac{\partial R_{sci}}{\partial Z}\Delta Z \quad . \qquad (1\text{-}37)$$

The coefficients of the form of partial derivatives in equation (1-37) correspond to the inverse of the direction cosine of calculated slant range R_{sci} with respect to X, Y and Z axes, respectively. By solving equation (1-37) using the ray path data of more than three observations, three unknowns (ΔX, ΔY, ΔZ) are estimated. These solutions are added to the initially estimated position of the sound source ($X's$, $Y's$, $Z's$). New initial position ($X''s$, $Y''s$, $Z''s$) becomes as

$$X''_s = X'_s + \Delta X \quad , \qquad (1\text{-}38)$$

$$Y''_s = Y'_s + \Delta Y \qquad (1\text{-}39)$$

and

$$Z''_s = Z'_s + \Delta Z \quad . \qquad (1\text{-}40)$$

This procedure is repeated until the solution reaches a threshold value. When equation (1-37) is solved, the least squares method is applied as well.

Chapter 2

2. Experiment

The ocean acoustic microtomography was proposed in the previous chapter. The method of theoretical approach was discussed. Unexpected problems concerning the software or the hardware, however, may remain. In order to make sure the feasibility of microtomography in the actual sea field, preliminary and verification experiments were carried out at sea.

When the actual experiment is made, the performance of system for tomography is important. The selection of navigational instruments for positioning and the propagation time measurement system of sound signal must be made while considering whether the accuracy of instrument satisfies the requirements for the microtomography.

In this chapter, the method, the instruments and the results obtained from the two-year experiments carried out at the Sagami Bay are mentioned.

2.1 Experiment (I) of 1991

The aims of this experiment are as follows: (1) The check of performance of the acoustic and the positioning measurement system, the confirmation of installation/recovery techniques and observation method. (2) The verification of plausibility of the inversion method

proposed. (3) The estimation of the mean vertical sound speed profiles by using the acoustic data between a transponder at the sea floor and the moving stations(transponders installed on board a vessel) at the sea surface.

2.1.1 Concept

Figure 2-1 shows the concept of instrumentation in 1991. It consists of two main systems. One is the micro wave positioning system and the other is the measurement system of sound propagation time.

The microwave positioning system(Trisponder, DEL NORTE, 542 Type, U.S.A.) is used for the positioning of the observation vessel. This system is composed of a master station installed on the vessel and two slave stations on land. A position of the vessel is calculated by using two distances between a master station and two slave stations.

The measurement system of sound propagation time is divided into a shipboard unit and an underwater unit installed on the sea floor. This is TRANS-NAVIGATION SYSTEM manufactured by KAIYO-DENSHI Co. Ltd, Japan. A round-trip propagation time of a pulsed sound signal between the transducer of the shipboard unit(this corresponds to the receiver at the surface in the previous chapter) and the underwater unit(this corresponds to the sound source on the sea floor) is measured. The influence of water current along a sound ray path can be nullified by measuring the round-trip propagation time. Instrumental details of the systems will be given in the later section.

The hydrographic observation was made by using the Conductivity Temperature Depth(CTD : NIEL BROWN, MARK III-B) measurement system and the Expendable Bathythermography(XBT : TSURUMI SEIKI, T5). The oceanic physical data obtained from these instruments

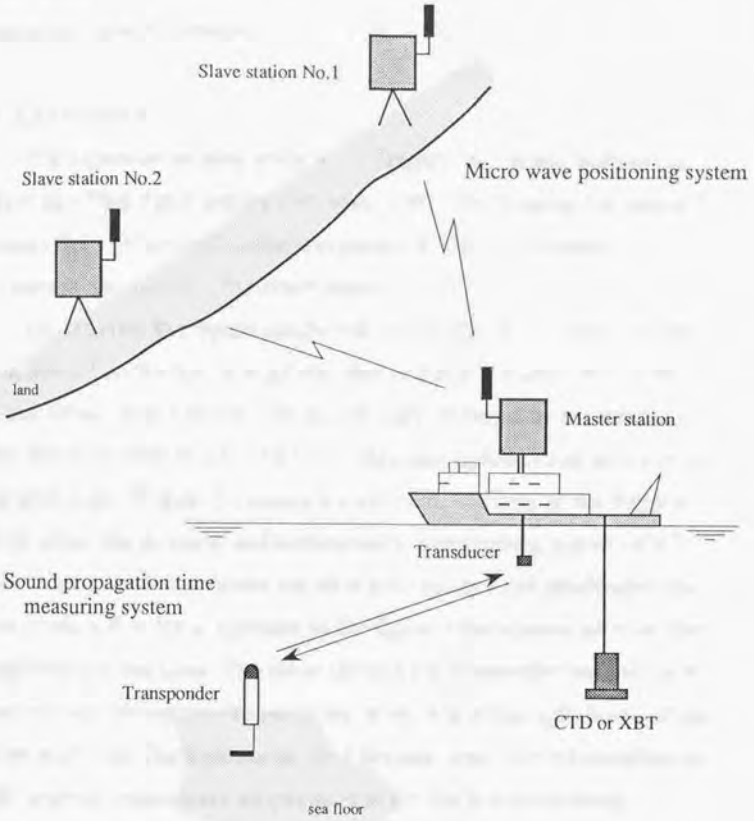

Fig. 2-1 Concept of experiment.

are used as reference data of the vertical structure of sound speed or sea temperature to be compared with the results from microtomographic analysis.

2.1.2 Method

The experiments were made at the Sagami Bay at the daytime on 21st and 22nd April and on 15th May, 1991. The training and research vessel Seiyo Maru(167 tonnage in gross) of Tokyo University of Fisheries was used for the experiment.

The Sagami Bay opens southward, so that the outer oceanic water circulates into the bay through the west and east channels besides the O-Sima Island. The water properties are easily affected by the change of the Kuroshio path in addition to the seasonal variation and intermixture of land water. Figure 2-2 shows the experimental area of the Sagami Bay where the acoustic and hydrographic observations were carried out. The sites of experiment are shown by an enclosed area(6 miles in longitude x 8 miles in latitude) in the figure. Observation areas of April and May are the same. The slave stations for Trisponder were set at the point of the Manazuru Peninsula and at the top of the light house of the Kawana Point. The location of slave stations were decided considering the angle of micro wave propagation to get the best positioning accuracy. The Sagami Trough with the depth larger than 1500 m runs through the center of the bay in the northwest-southeast direction and its northern end reaches off Manazuru Peninsula. A terrace of 1000 m to 1500 m depth developed at both sides of the trough, where the underwater transponder was installed. The depth was 1350m.
The slope of landward shelf east of the Izu Peninsula is especially steep and the maximum slope amounts to about 16 degrees

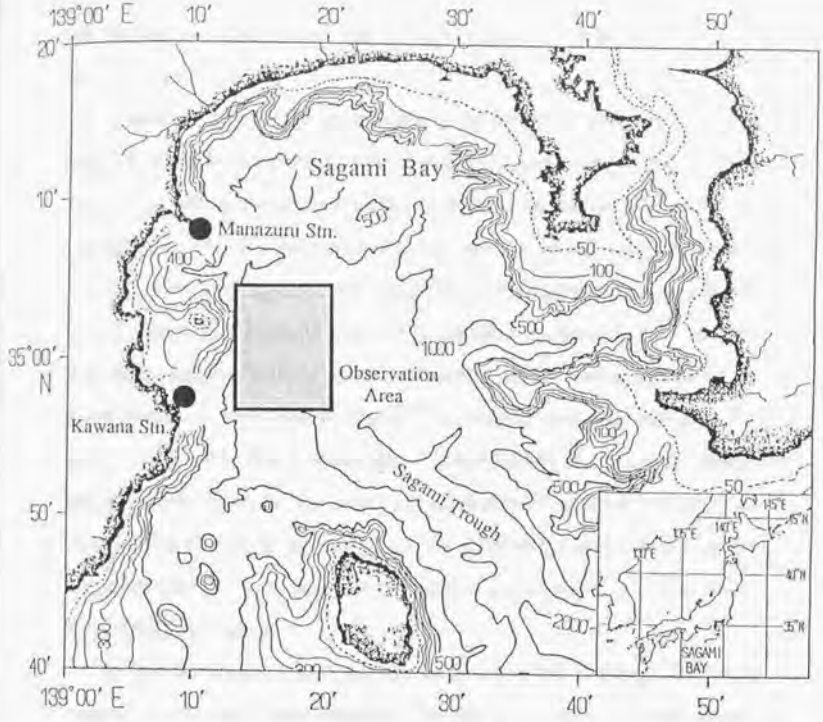

Figure 2-2 Observation area(enclosed) at the Sagami Bay in April and May, 1991.

off the Hatsu-Sima Island. The western most end of the observation line reaches this slope.

Figure 2-3 shows the locations of experiment station in April and May. The stations marked by circles are located along three north-south lines. The transponder on the bottom was set in the middle of the central line. The distance from the central line to the side lines is about 3 miles. The spacing between two successive stations on a line are from 1 to 2 miles. The stations total 21 in number in April and 27 in May. The hydrographic observations were made at the stations marked by the solid circles in each figure. The CTD observations were made at 7 stations in April. The hydrographic observations in May were made by the XBT only because the sound speed dependency on the salinity and its monthly variation are small. As the XBT measurement is a quick measurement the total number of stations increased to 27 when the XBT stations were 9.

At the observation stations, the vessel was left drifting. The main engine of the vessel was stopped. The sub-generator only was working for the sake of the power for the instruments. The acoustic noises radiated omnidirectionally from the vessel to water cause degradation of S/N ratio. The problem of noise reduction is very important for the acoustic observation. In order to reduce the radiation noise the cable length of the transducer of the onboard unit was made 5 m below the surface.

The measurement starts by transmitting an acoustic pulse from the transducer. When the signal is received by the transponder installed on the bottom, it returns another signal towards the vessel. The time for the acoustic pulse to make a round-trip is measured by the receiver installed onboard.

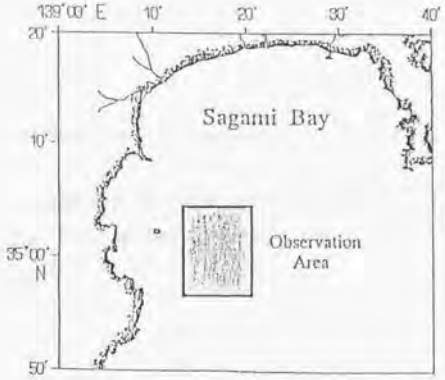

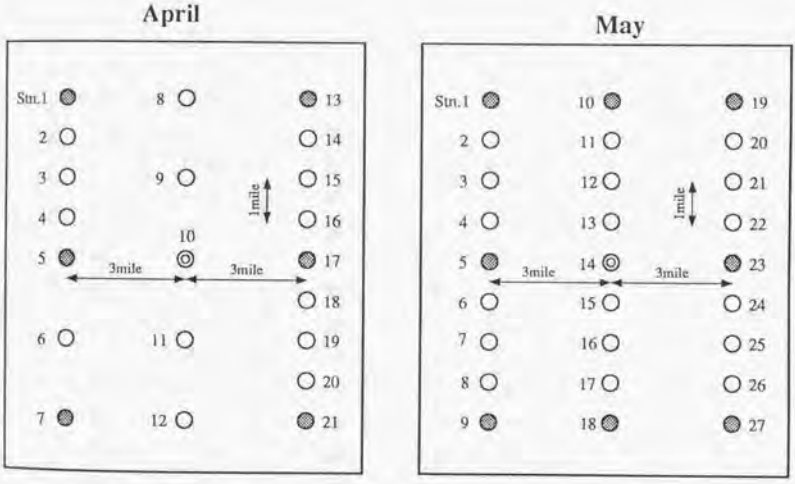

◎ Station right above the point of acoustic transponder on the bottom, where sound propagation time and CTD or XBT were made.

○ Stations where sound propagation time was measured.

● Stations where sound propagation time and CTD or XBT were measured.

Fig. 2-3 Configulation of the stations of experiment in April and May, 1991.

Table 2-1(a) Summary of observation in April,1991

Station No.	Horizontal range (km)	No.of transmission of acoustic signal	SD of propagation time error (ms)
1	9.6	21	---
2	8.2	22	1.3
3	6.8	20	0.7
4	6.5	21	1.0
5	6.3	22	1.4
6	7.6	23	0.9
7	9.2	20	---
8	7.5	15	---
9	2.7	25	1.2
10	1.5	39	1.1
11	2.5	31	0.9
12	7.4	20	---
13	9.4	28	---
14	7.3	21	1.9
15	6.0	22	1.1
16	5.0	23	1.0
17	4.2	22	0.9
18	5.1	25	1.3
19	6.2	23	0.8
20	7.6	24	1.5
21	9.0	20	---

Horizontal range : Horizontal range between transponder at the sea floor and station.

Table2-1(b) Summary of observation in May, 1991

Station No.	Horizontal range (km)	No.of transmission of acoustic signal	SD of propagation time error (ms)
1	9.0	20	---
2	8.1	18	0.9
3	6.6	19	1.0
4	5.7	15	1.3
5	5.5	18	1.2
6	5.7	22	1.0
7	6.7	23	0.8
8	8.1	21	1.1
9	9.2	20	---
10	7.8	26	1.5
11	5.7	19	1.0
12	4.0	18	1.6
13	1.9	18	1.2
14	0.2	27	0.9
15	1.6	24	1.0
16	3.4	19	0.9
17	5.3	18	1.3
18	7.3	17	1.8
19	9.1	28	---
20	8.3	18	1.1
21	7.1	21	1.4
22	6.3	19	0.7
23	6.1	28	1.4
24	6.3	21	1.5
25	7.2	20	1.7
26	8.4	34	---
27	9.3	20	---

Horizontal range : Horizontal range between transponder at the sea floor and station.

The interval of transmission of the acoustic pulses was set 20 sec to 30 sec. This interval was selected considering the round-trip propagation time of the signal. The repetition of transmission from a station was from 15 to 39 times. The total number of transmission of acoustic pulses became finally 487 in April and 571 in May. The vessel's coordinates measured by the Trisponder were sampled every 1 sec during the experiment. The coordinates(X, Y, 0) in meter of the vessel is expressed in the relative coordinate system with the origin(0, 0, h (height)) which is set at the Kawana land station.

Table 2-1(a) and Table 2-1(b) show the summary of experiments: the averaged horizontal range between the transponder on the sea floor and the station at surface, the number of transmissions and standard deviation(SD) error of measured propagation time in April and in May. The sea condition was comparatively good throughout the experimental period. The mean wind speeds in April and May were 4.0 m/sec and 2.0 m/sec, respectively. The data of propagation time could not be measured at the stations No.1, 7, 13 and 21 in April and No.1, 9, 19 and 27 in May where the horizontal ranges exceeded 9 km. This limitation of propagation is related to the vertical structure of the sound speed and the transmission level of the transponder. The total average of SD error of propagation time was 1.14ms in April and 1.21msec in May.

2.1.3 Instrumentation

[Microwave positioning system(Trisponder)]

Figure 2-4 shows the block diagram of the Trisponder (DEL NORTE, 542 Type DDMU(Digital Distance Measurement Unit)) and the principal specifications. The distance between a master station and a

slave station is calculated from the measured propagation time of synchronized pulse signal of microwave. A position of master station is calculated by using two or more distance data , i.e., by ρ-ρ navigation. This type DDMU can simultaneously receive and process 8 signals from different slave stations. The positioning accuracy of the master station in a stationary condition like the fixed point observation is higher than about 30 cm. The accuracy is higher than 1 m in a moving condition. The resolution is 0.1 m. The accuracy of 1 m seems to be the best among the dynamic positioning methods available at sea.

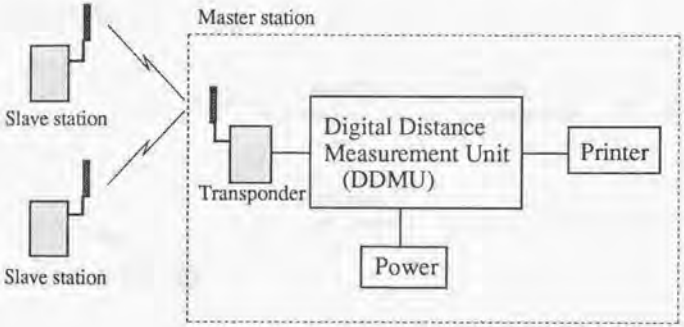

Principal specifications

Measuring range	: 75m ~ 80km
Ranging accuracy	: 1m
Resolution	: 0.1m
Source power	: 22 ~ 27 VDC, 1.9A

Fig. 2-4 Block diagram of the microwave positioning system and the principal specifications

The antenna of master station on board the Seiyo Maru was installed at the upper deck, and the antennae of the slave stations were fixed on a tripot (Manazuru) or at the handrail of the light house (Kawana). The

power of DC 24 V was supplied to the slave units from a battery. The heights of antenna from the sea level was 43 m at Manazuru and 47 m at Kawana. Photo.1 shows the 542 type DDMU. Photos.2 and 3 show the slave units at Manazuru and Kawana.

[Measurement system of sound propagation time]

Figure 2-5 shows the block diagram of the measurement system of the sound propagation time designed for the microtomography and the principal specifications.

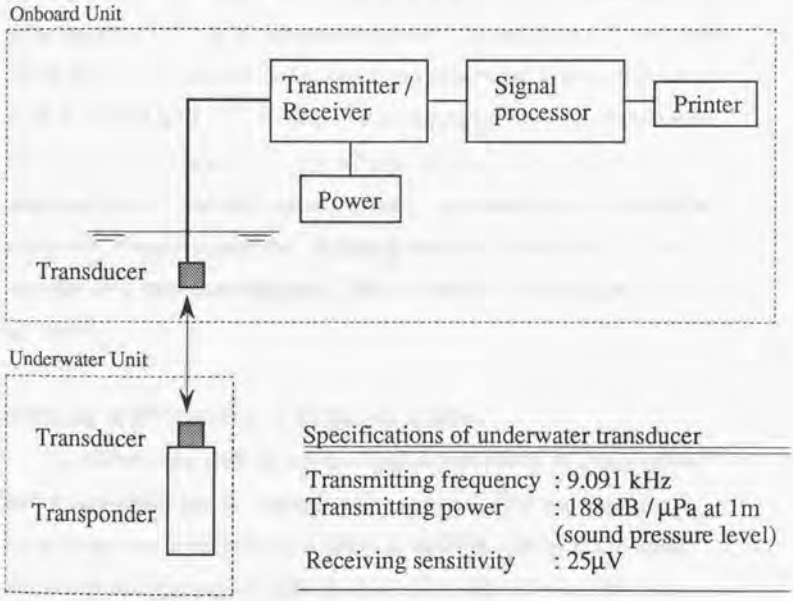

Fig. 2-5 Block diagram of the measurement system of sound propagation time and the principal specifications of underwater transducer.

This system can also be used for the LBL(long-baseline) acoustic navigation (Fujimoto et al,1988; Furuta et al,1984). The shipboard unit is composed of transmitter/receiver, signal processor and transducer. The transmitter/receiver and the signal processor are shown in Photo.4. The transducer is shown in Photo.5. The shipboard transducer is usually suspended from the side of the vessel.

The command signals(Active, Passive and Release) coded by FSK(frequency-shift keying) modulation are generated by the command generator and the pulse signal of 0.25 sec width and 9.091kHz for the measurement of propagation time is generated by the pulse generator of the transmitter/receiver. A transmitting interval and the timing of the acoustic pulse can be set manually. The transmission level is 188 dB/μPa at 1 m. The responded pulse from the transponder on the sea floor is received by the transmitter/receiver circuit, amplified up to a suitable signal intensity, and transferred to the signal processor. The processed data is finally output to a printer, a X-Y recorder or a personal computer. The resolution of propagation time is 0.1 msec.

[Mooring of the transponder on the sea bottom]

The underwater unit on the sea floor is composed of a transponder with a transducer and an acoustic release device. The unit weights 11 kg in water and the operational depth is 6000 m. The unit has three electronic circuits: command/signal receiver, signal transmitter and a release for self-surfacing. Photo. 6 shows the transponder.

Figure 2-6 shows the mooring system of the underwater unit. The weight of 100 kg is attached to the end of bottom side of the mooring system. The transducer is suspended 12 m above the weight. Two glass

Photo. 1 Digital distance measurement unit(542 type) of Trisponder system.

Photo. 2 Slave station of Trisponder system set at the Manazuru.

Photo. 3 Slave station of Trisponder system set at the Kawana Light House.

Photo.4 Transmitter/receiver and signal processor of shipboard unit

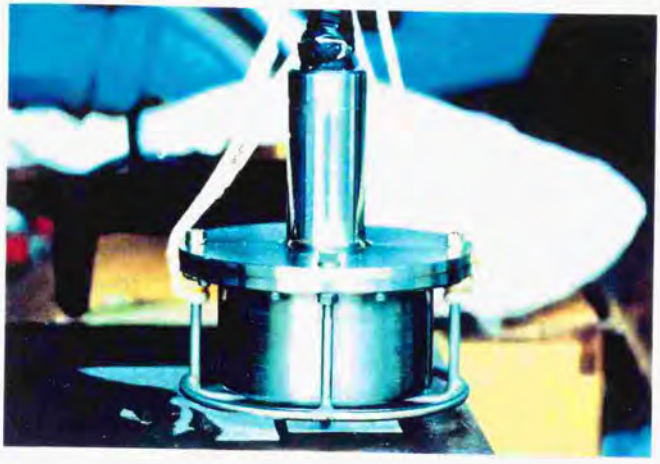

Photo.5 Transducer of shipboard unit

Photo.6 Transponder

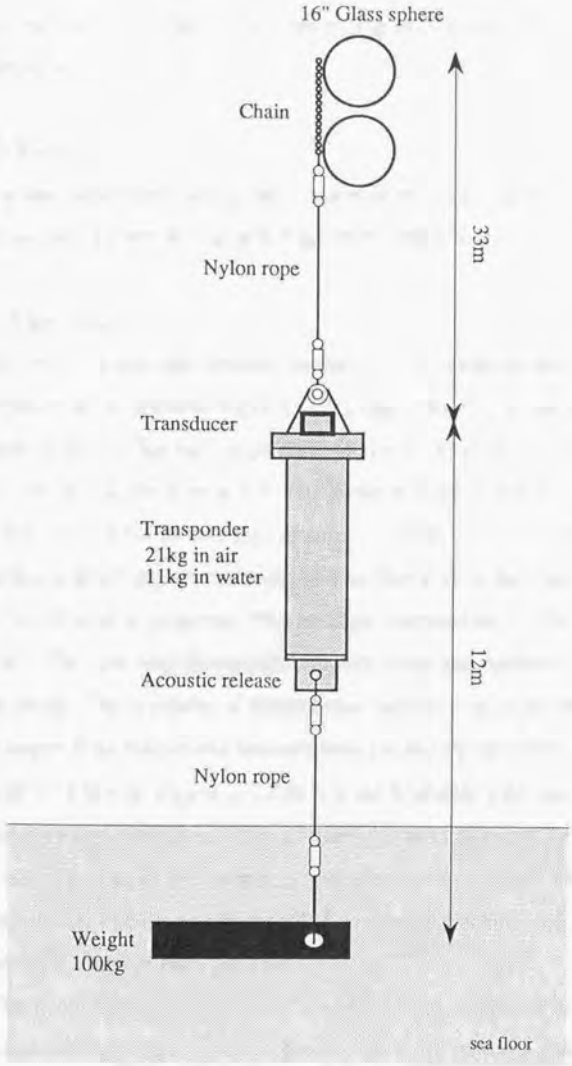

Figure 2-8 Mooring system of transponder

spheres used for the surfacing are attached to the top of the system. Some swivels are inserted at the connecting points of each rope and the transponder.

2.1.4 Results

The results of the hydrographic observation made in April and May at the stations shown in Figure2-3 are mentioned here.

April Experiment

Figure 2-9 shows the vertical profiles of the averaged sea temperature(left), salinity(middle) and sound speed(right) as a function of depth in April. The data were obtained by CTD system at seven stations shown in the Figure 2-3. The surface mixed layer was seen from surface to 10 ~ 20 m depth at some stations. The surface temperature at the experiment area shows that it is in the transition period from winter to spring. The average temperature at the surface is 15.8 °C. The principal thermocline is seen from the surface to about 500 m depth. The gradient of temperature begins to decease at the depth larger than 500 m and the temperature finally becomes 2.5 °C at the deph of 1364 m. Figure 2-10 shows the Kuroshio path near the Sagami Bay and surface sea temperature contours of every 2 °C in the observation period in April(upper) and May(lower), 1991. This temperature distributions are regarded as normal because the Kuroshio axis runs offshore in both periods.

The low salinity of 34.33 ‰ and 34.24 ‰ appeared at the surface at stations 1 and 5 where the locations are near the coast of the Izu Peninsula. The salinity of other stations at the surface varies slightly about 34.5 ‰. The maximum(34.54 ‰) and the

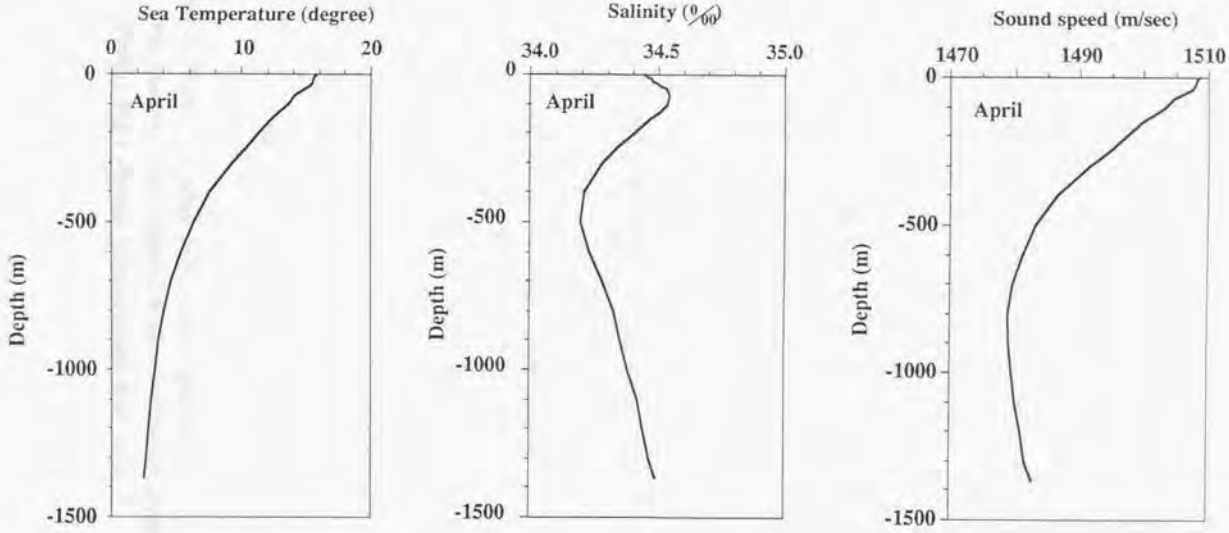

Figure 2-9 Vertical profiles of averaged sea temperature(left), salinity(middle) and sound speed(right) in April, 1991.

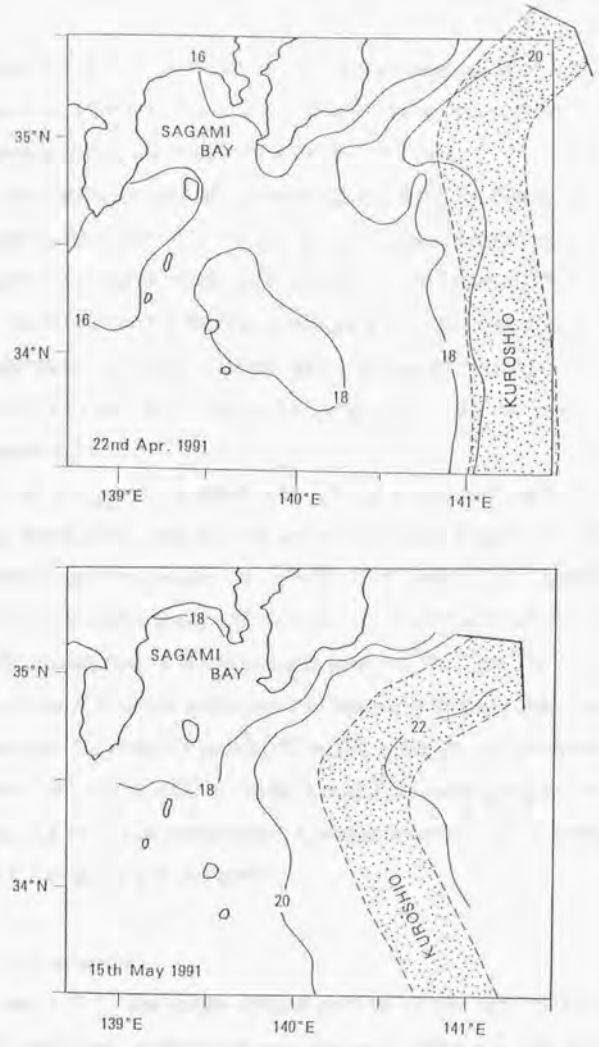

Figure 2-10 The Kuroshio paths near Sagami Bay in April(upper) and in May(lower), 1991. (based on the data from Kanagawa Prefectural Fisheries Experimental Station)

minimum(34.19 ‰) of the salinity in the averaged profile of Figure 2-9 correspond to the depths of 75 m and 500 m, respectively. This pattern is the typical one seen at the Sagami Bay.

The sound speed profiles were derived from the Mackenzie's equation(see equation (1-3)) using the measured temperature and salinity. The sound speed shows the maximum value of 1508.6 m/sec at the sea surface and it decreases rapidly due to the lowering of sea temperature up to 800 m depth, where the speed becomes the minimum of 1478.9 m/sec. Then, the sound speed turns to the increase due to the pressure effect.

Although the parameters of sea water vary with stations in the experiment area, their scatters are not so large. Figure 2-11 shows the variations of standard deviation(SD) of the scatters of temperature, salinity and sound speed with stations as a function of depth observed in April. Fluctuation of salinity is less than 0.1 ‰. The SD of temperature is larger in the layer of the main thermocline. The maximum SD amounts to 0.51 °C at 150 m depth, and it becomes less than 0.1 °C below 1000 m depth. The SD of sound speed shows the same pattern as the temperature. The maximum SD of the sound speed was 1.7 m/sec at 150 m depth.

May Experiment

Figure 2-12 shows the vertical profiles of averaged temperature, and sound speed observed at nine stations in May. The mixed layer at the sea surface observed in April disappeared in May and the thermocline became significant. The maximum temperature was 17.4 °C at the surface. The temperature decreases rapidly up to the depth of

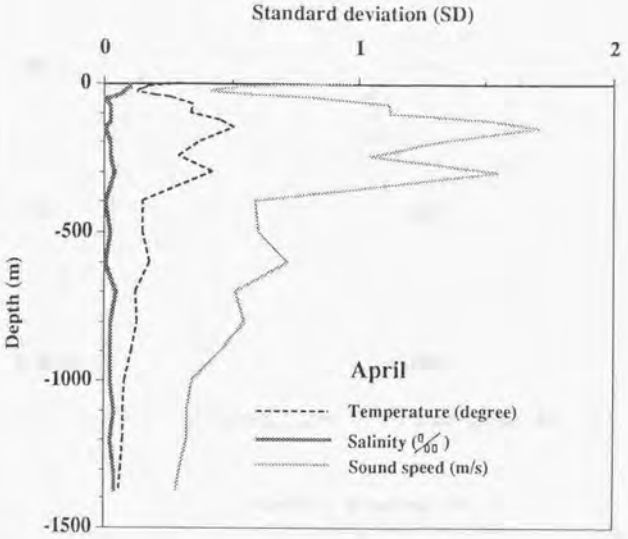

Figure 2-11 Variations of standard deviation of the scatters with stations of temperature, salinity and sound speed as a function of depth in April, 1991.

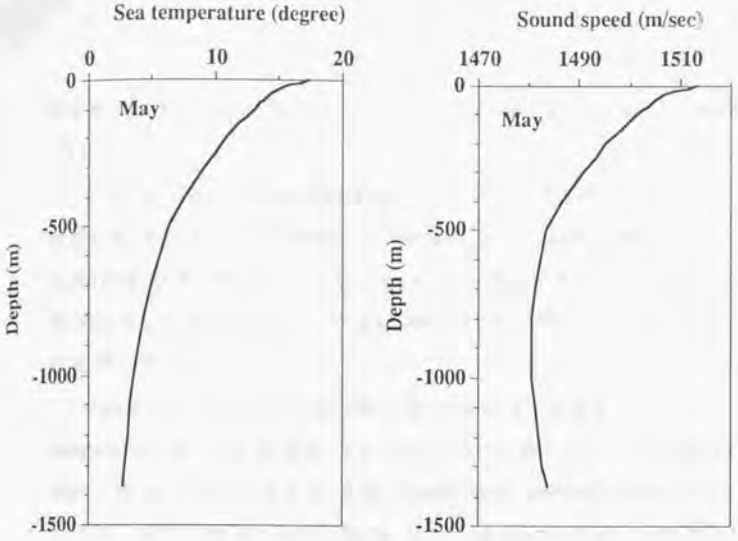

Figure 2-12 Averaged temperature and sound speed observed in May, 1991.

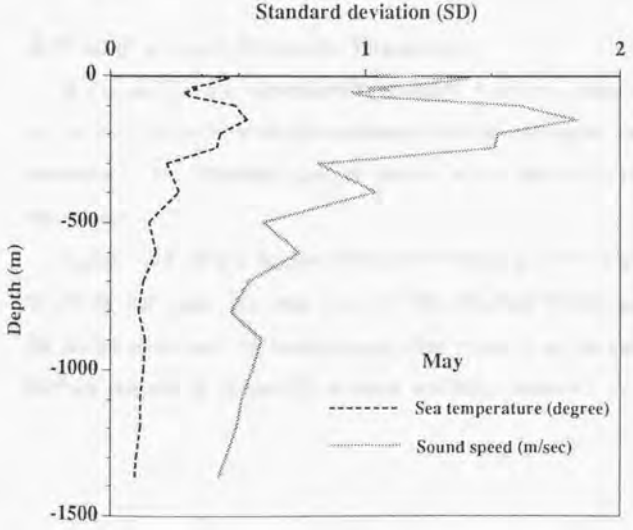

Figure 2-13 Standard deviation of the scatters with stations of temperature and sound speed as a function of depth observed in May, 1991.

500 m like in April. The lowest temperature was 2.8 °C at the depth of 1364 m.

The sound speed decreases steeply from 1513.4 m/sec (maximum) at the surface to 1480.5 m/sec (minimum) at the depth of 900 m according to the decrease of temperature with depth. The sound speed increases gradually due to the pressure effect from the depth larger than 900 m.

Figure 2-13 shows the standard deviation of the scatters of temperature and sound speed with stations as a function of the depth in May. The maximum of SDs of the temperature and the sound speed are 0.54 °C and 1.8 m/sec at the depth of 150 m, respectively, similarly with the case of April. Both SDs become small with depth and finally approaches 0.1 °C and 0.4 m/sec at depth of 1364m.

Estimation of Sound Speed and Temperature

In this section the experimental settings of acoustic data acquisition for the estimation of vertical structure of the sound speed and the temperature are described and the results of estimation by inversion are mentioned.

Figure 2-14 shows the stations (solid circle) of April and May where the acoustic data were successfully obtained for the estimation of the sound speed and the temperature. The numbers of the successful stations amount to 14 and 21 in April and May, respectively.

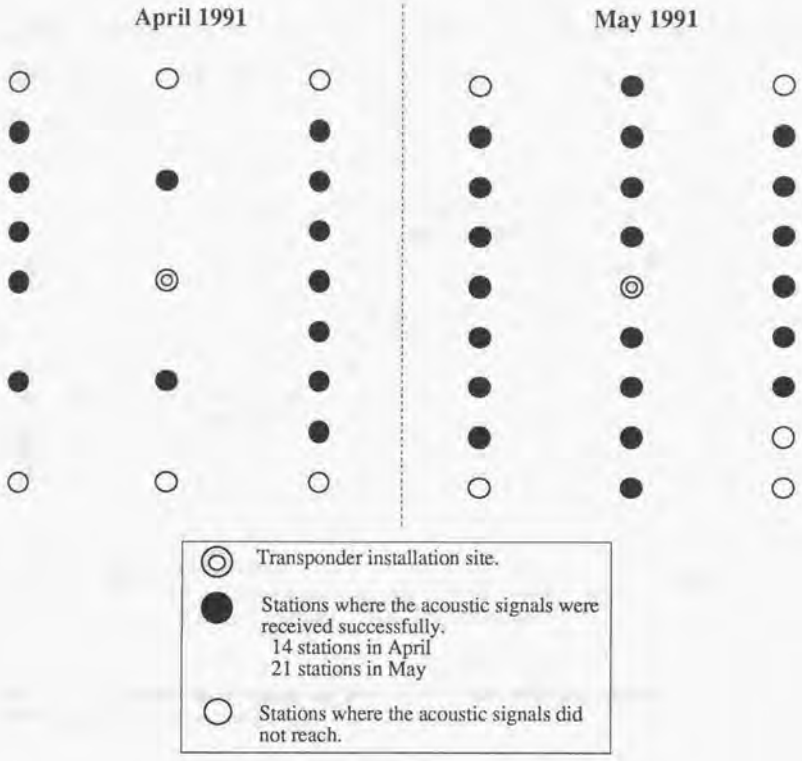

Figure 2-14 Distribution of stations used for the sound speed estimation. .

Using these data, the mean vertical structure in the area concerned(6km east-west by 15km north-south) are estimated. The data of sound propagation time were not obtained at stations of the numbers 1, 7, 13 and 21 in April and the number 1, 9, 19 and 27 in May(see Figure 2-3 and Table 2-1(a) and 2-1(b)). This is because the stations were located too far from the transponder. As illustrated in Figure 2-15, the horizontal ranges for which the total reflection of sound ray at the sea surface occurs are 8983 m when the upward transmission angle

is θ=79.4 degrees in April and 8579 m when θ=79.2 degrees in May. These ranges impose the receivable limitation on the acoustic signal at the surface.

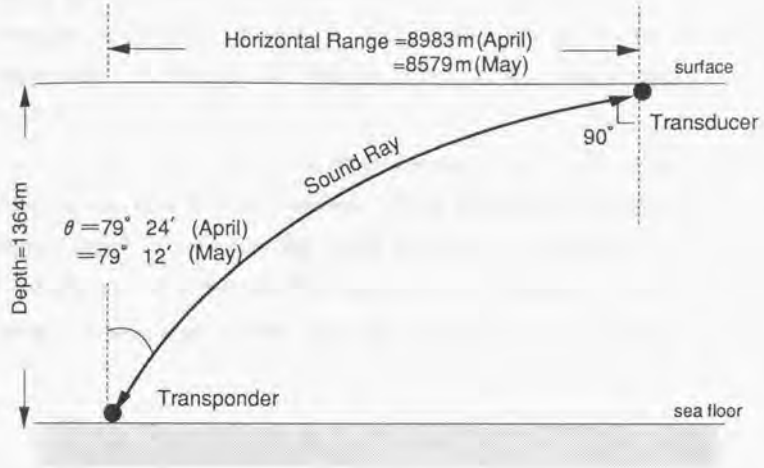

Fig. 2-15 Illustration of sound ray in case the total reflection occurs at the surface in April and May.

Figure 2-16 shows the sound speed profiles of the observed(Vo) and the estimated(Vc) by 10th degree Chebychev polynomial(left) and the estimation error[Vc - Vo] profile(right) for April. The error of estimation of the sound speed was -0.37 m/sec in average and 1.08 m/sec in standard deviation(SD). Figure 2-17 shows the profiles of observed(to) and estimated(tc) sea temperature(left) and the error profiles of [tc - to] (right) for April. The temperature tc is converted from the data of estimated sound speed(Vc) in Figure 2-16 using Mackenzie's equation (1-3). The average and SD of [tc - to] were -0.13 ^{o}C and 0.29 ^{o}C, respectively.

Figure 2-18 shows the profiles of the observed(Vo) and the estimated(Vc) sound speed(left) and the error[Vc - Vo] profile(right) for May. The errors were -0.40 m/sec in average and 1.09 m/sec in SD. Figure 2-19 shows the profiles of temperature of observed(to) and estimated(tc)(left) and, the profile of estimation error [tc - to] for May(right). The average and SD error of [tc - to] was -0.12 ^{o}C and 0.33 ^{o}C.

The results from the preliminary experiment mentioned above have demonstrated the performance of the acoustic measuring system and the feasibility of estimating sound speed structure by means of Chebychev polynomials. Further application of microtomographic techniques was made in 1992 under different settings as Experiment II.

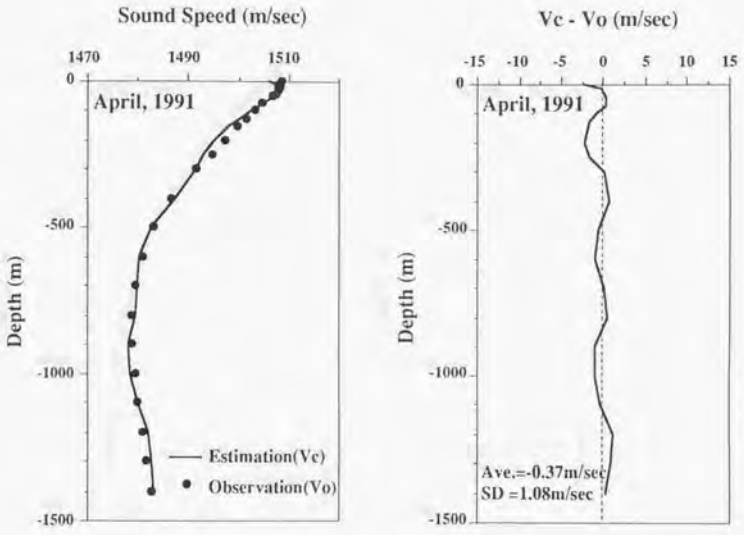

Figure2-16 Comparison between estimated and observed sound speed profiles for April, 1991.

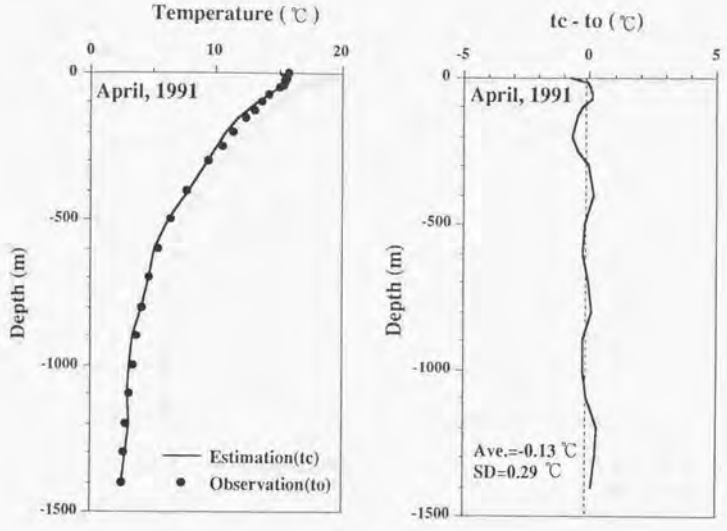

Figure 2-17 Comparison between estimated and observed temperature profiles for April, 1991.

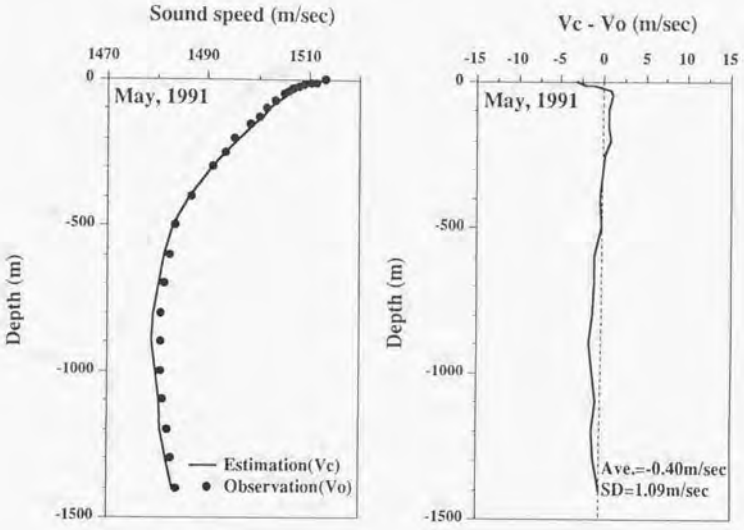

Figure 2-18 Comparison between estimated and observed sound speed profiles for May, 1991.

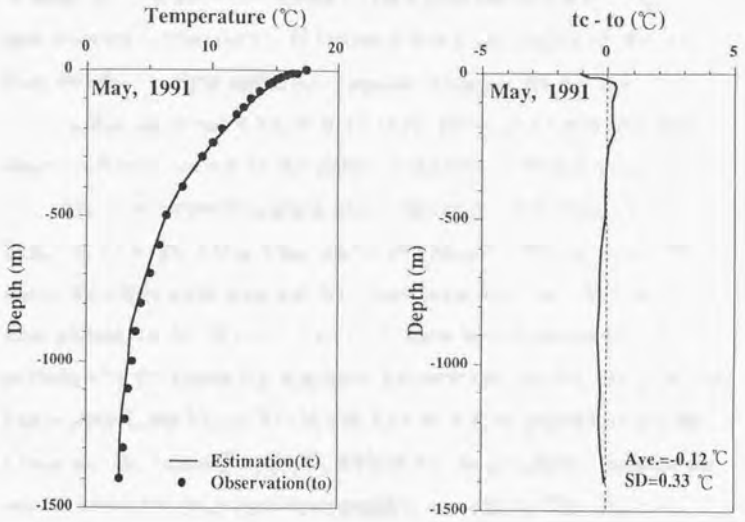

Figure 2-19 Comparison between estimated and observed temperature profiles for May, 1991.

2.2 Experiment (II) of 1992

2.2.1 Concept and Method

The purposes of this experiment are: (1) Verification experiment for the practical use of microtomography in the future. (2) Estimation of areal mean of the sound speed and temperature profiles using the acoustic propagation time data between four transponders on the sea floor and the multiple stations(transponders) at the sea surface.

In this experiment the method of the previous experiment was almost followed except for the points described in the following.

The experiment was made in the area east of the Hatsu-Sima Island in the Sagami Bay from 2nd to 6th March, 1992. Figure 2-20 shows the experiment area and the observation stations. The stations were plotted on the 'Western Part of Sagami Wan Bathymetric Chart' published by the Japan Hydrographic Department. Double circles at the Hatsu-Sima Light House(35-02.1'N, 139-10.6'E, height=63m) and the Kawana Light House(34-57.1'N, 139-08.9'E, height=54m) indicate the slave stations for the micro wave positioning system. The master station was set on a fishing boat(Moriryu-Maru, 15 tonnage in gross) and the position of the ship was measured every 1sec. The solid circles A, B, C and D in Figure 2-20 show the positions of the acoustic transponders installed on the sea floor. These transponders were at the depth from about 1300m to 1400m and the separations between them were 1.6km in average. The mooring of the transponder was the same as at the experiment of 1991. The solid triangles(No.1 ~ No.9) show the observation stations where the sound propagation time was measured. The transducer of the onboard unit was suspended from the ship side by a cable of 5m. The observations were made mostly above the bathymetric slope so as to investigate the effect of the slope on the sound propagation. The measurement of propagation time at the

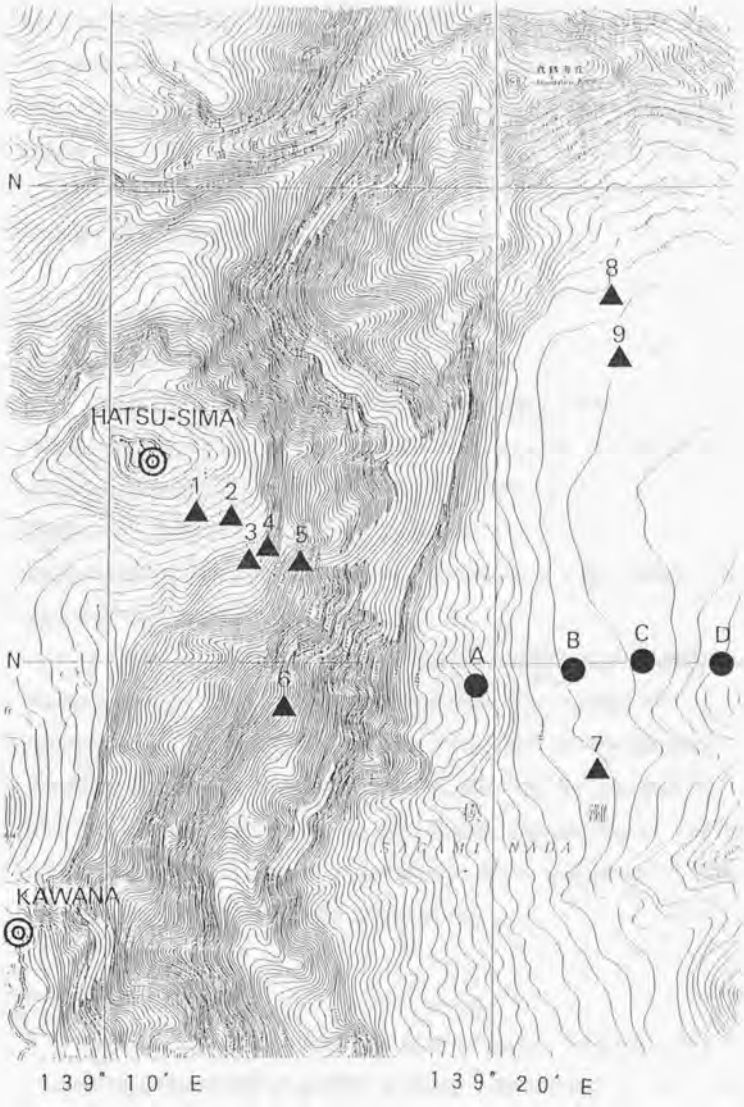

Figure 2-20 The experiment area of March, 1992 and the observation stations.

stations was made while the ship was drifting. The interval of transmission was 20sec and the number of transmission at a station amounted to 11 ~ 69. The onboard receiver can receive and process signals from four transponders A, B, C and D at a time. The XBT observations were made at stations 7 and 8 and at sites just above transponders C and D.

2.2.2 Results

Observed Sea Temperature

Figure 2-21 shows the Kuroshio path and the surface sea temperature contour every 2 °C around the Sagami Bay on 4th March. 1992 based on the Kanagawa Prefectural Fisheries Experimental Station. A small scale meander of the Kuroshio path was seen at the eastern area of the Izu Islands. The sea temperature at the Sagami Bay was regarded normal.

Figure 2-22 shows the averaged profiles of sound speed(left) and the temperature(right) observed at four points. The scatters of temperature among the XBT drop sites were small and the standard deviation at each depth was within 0.1 °C, showing the structure of temperature was stable during the experiment. The development of the mixed layer in the shallow part above 120m depth was observed. This profile is considered as typical in mid winter.

Propagation Time

Table 2-2 shows the summary of observation in March, 1992. The average horizontal range(HR) between a station and a transponder, number of transmission(n) and the standard deviation(SD) of the error of measured propagation time at each station are listed in the table. The SD fell within 0.3 ~ 1.6msec except for four combinations of (1)station

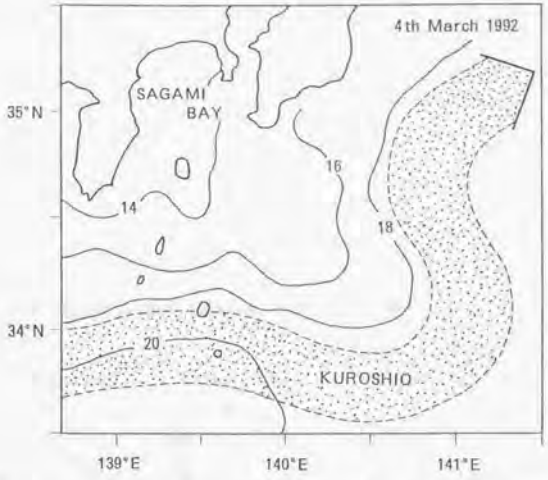

Figure 2-21 The Kuroshio path and the surface sea temperature contour every 2 °C around the Sagami Bay on 4th March, 1992 (After Kanagawa Prefectural Fisheries Experimental Station).

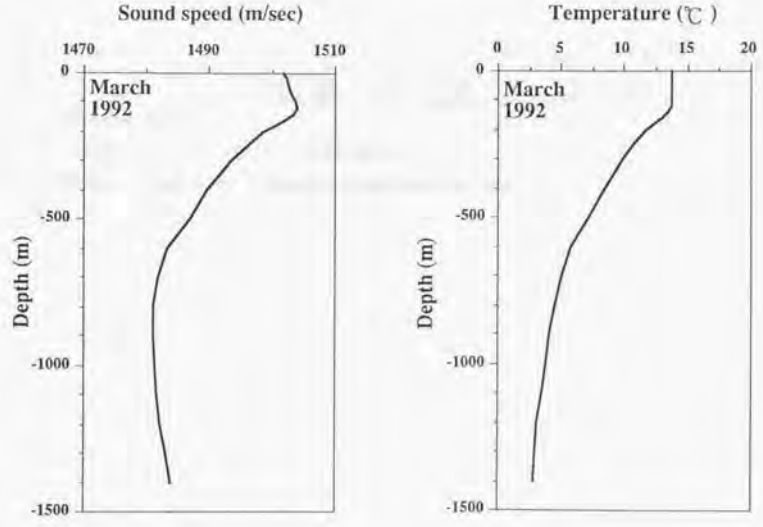

Figure 2-22 The averaged profiles of sound speed(left) and the temperature(right) observed at four points.

Table 2-2 Summary of observation in March, 1992

Station No.	Transponder A			Transponder B			Transponder C			Transponder D		
	HR	n	SD	HR	n	SD	HR	n	SD	HR	n	SD
1	6.3	11	30.1	8.0	11	1.0	9.2	11	0.6	10.8	20	---
2	5.8	30	1.6	7.4	54	1.1	8.5	54	1.3	10.1	24	---
3	5.1	10	0.3	6.9	24	1.5	8.1	24	0.7	9.7	14	20.4
4	4.8	25	1.4	6.5	38	0.9	7.7	38	1.3	9.2	13	0.5
5	4.1	22	1.4	5.8	51	1.3	7.0	51	1.1	8.5	29	1.3
6	3.8	34	0.6	6.0	69	0.9	7.3	69	1.1	8.9	35	1.6
7	3.1	26	0.9	2.1	50	1.1	2.5	50	0.9	3.3	24	0.9
8	7.8	17	1.0	7.7	35	1.5	7.5	35	0.7	7.8	18	1.2
9	6.6	26	1.5	5.9	56	1.3	5.7	56	1.1	6.1	30	1.4

HR : Horizontal range (km)

n : Number of transmission of acoustic signal

SD : Standard deviation of the error of propagation time (ms)

1- transponder A, (2)station 1 - transponder D, (3)station 2 - transponder D and (4)station 3 - transponder D. In the case of (2) and (3) the acoustic signal was not received and in case (4) the signal was unstable. The horizontal ranges for this case were 10.8 km, 10.1 km and 9.7km. The horizontal range occurring the total reflection at the surface, which was calculated from the sound speed profile observed in this experiment, is about 13.5km. Judging from this the receivable range of transponder system used in this time seems to be about 10.0 km. The large SD of 30.1msec was observed in case (1). It may have been caused by the offshore slope because the horizontal range is short enough to be within the receivable range. The signals must have been weakened and became unstable due to the interruption of propagation by the irregular slope.

Figures 2-23 through 2-31 show the distribution of propagation time measured at each station(station No.1 ~ No.9) as a function of horizontal range between a station and a transponder. A, B, C and D shown in the figure are corresponding transponders of Figure 2-20. The upper parts of the figures show the propagation time between a certain receiving station and transponders A, B, C and D . The lower parts of the figures show the enlarged plots of the upper figure with each transponder. The scale of horizontal and vertical axes varies with each plot enlarged.

Estimation of Sound Speed

The estimation accuracy of sound speed/sea temperature is described in this section. The number of data of propagation time determined by the number of combination of a station and a transponder, and also the degree of the Chebychev's polynomial are taken into consideration in this case. Table 2-3 shows the estimation

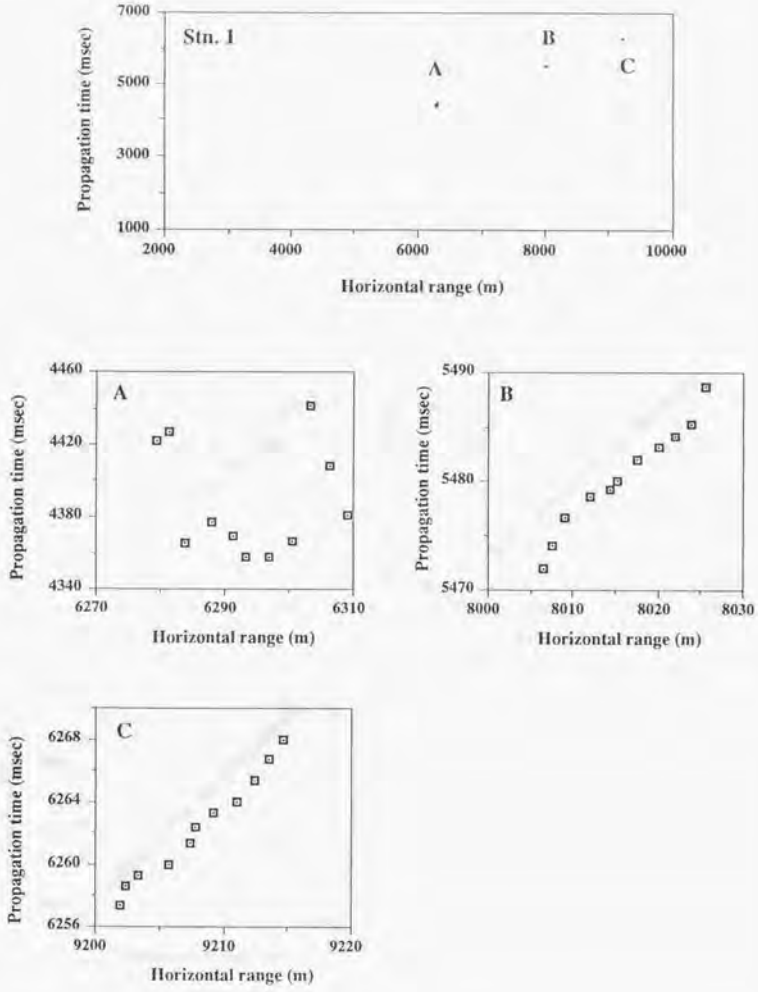

Figure 2-23 Propagation time from transponder A, B, C and D as a function of horizontal range between station 1 and transponders.

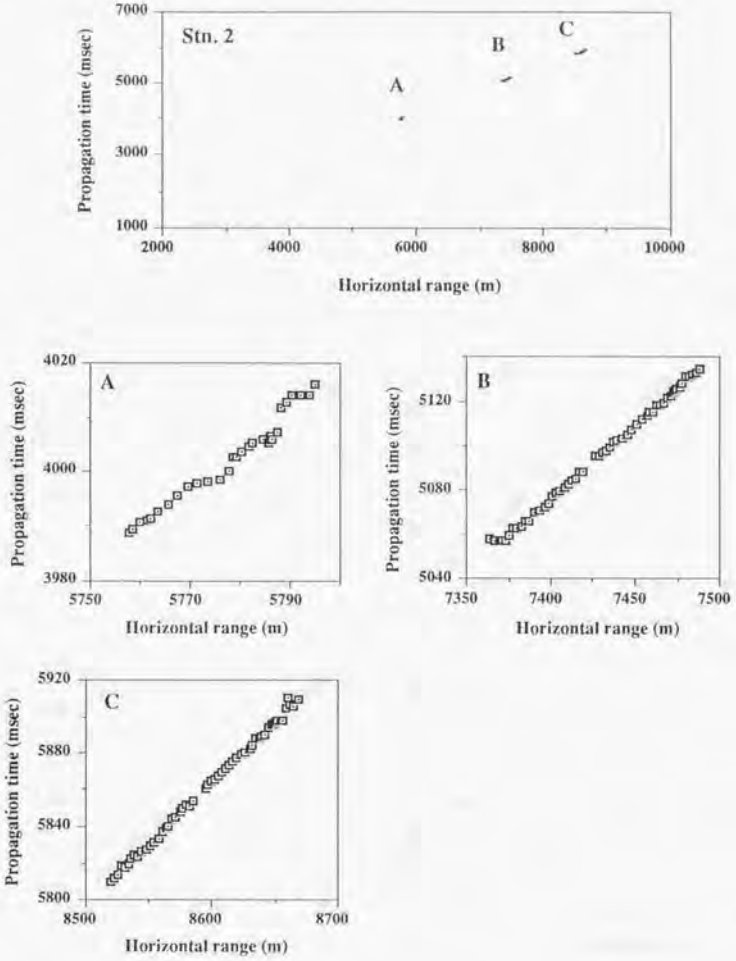

Figure 2-24 Propagation time from transponder A, B, C and D as a function of horizontal range between station 2 and transponders.

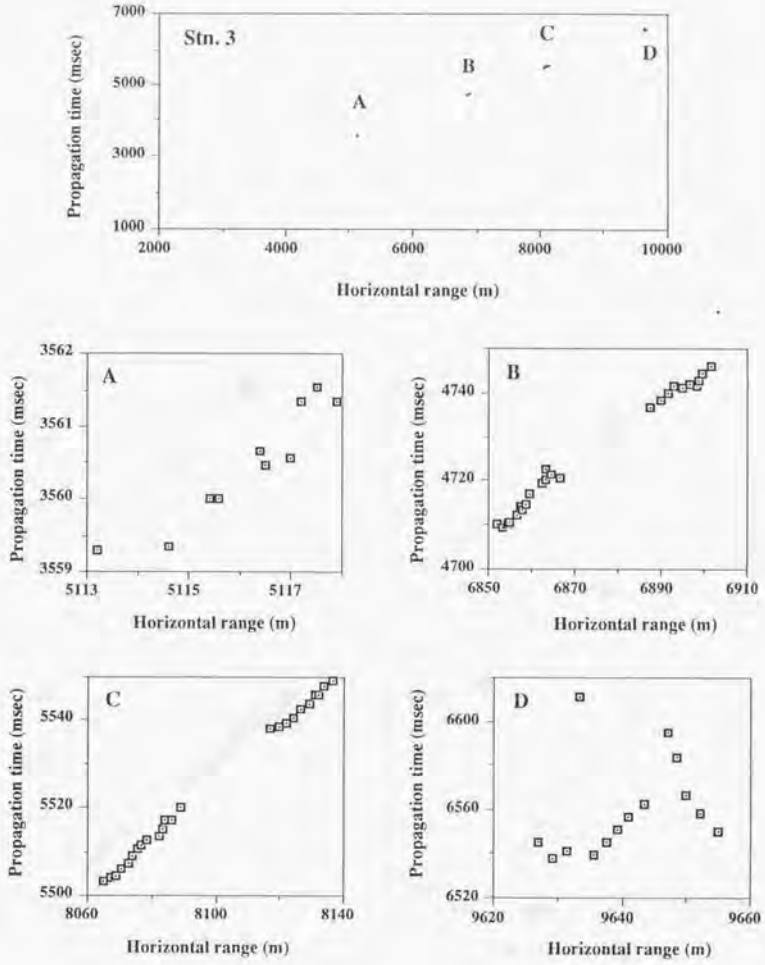

Figure 2-25 Propagation time from transponder A, B, C and D as a function of horizontal range between station 3 and transponders.

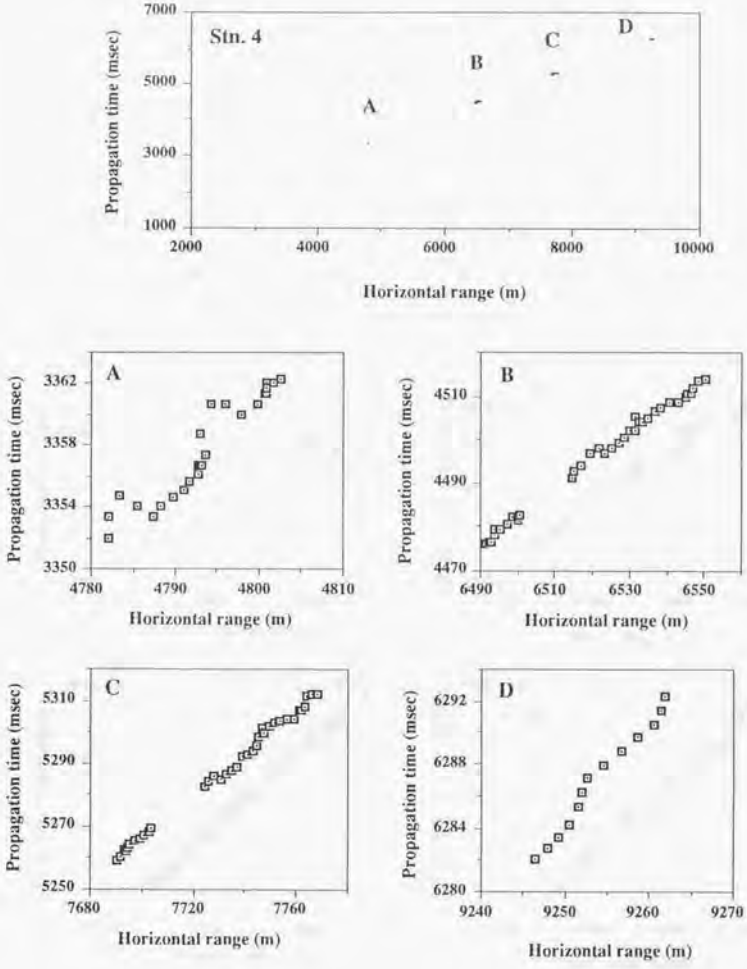

Figure 2-26 Propagation time from transponder A, B, C and D as a function of horizontal range between station 4 and transponders.

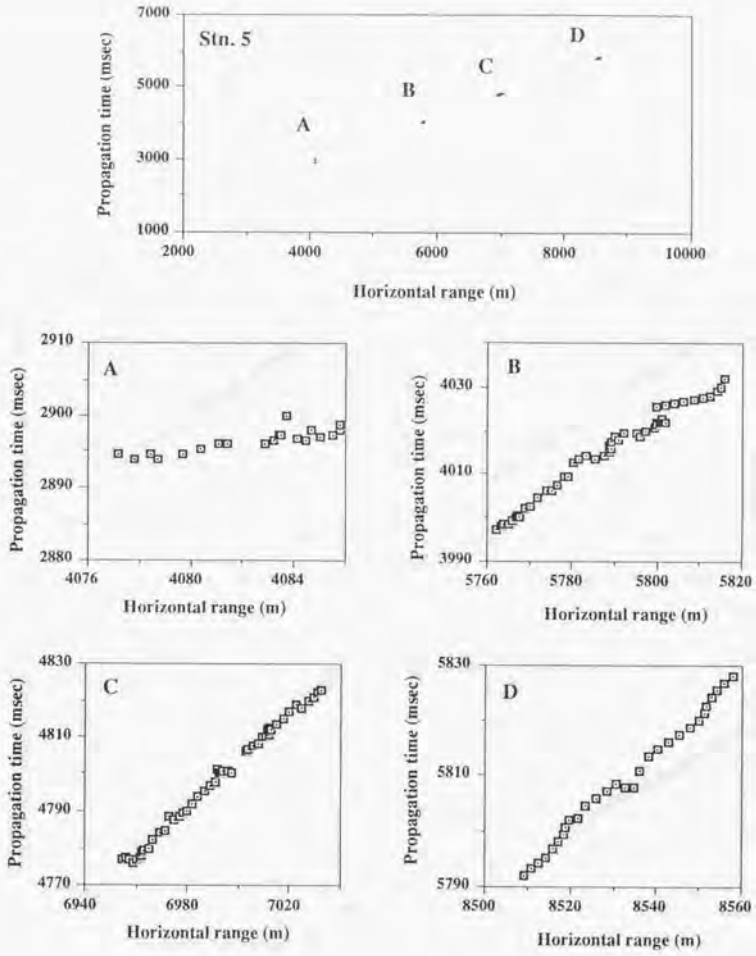

Figure 2-27 Propagation time from transponder A, B, C and D as a function of horizontal range between station 5 and transponders.

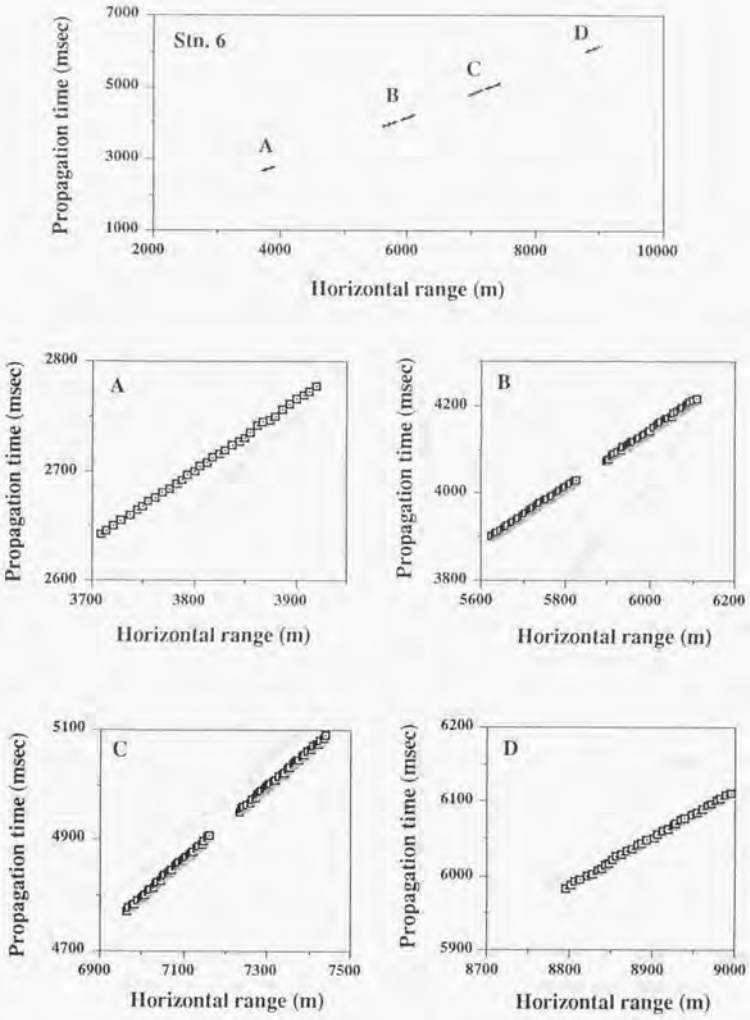

Figure 2-28 Propagation time from transponder A, B, C and D as a function of horizontal range between station 6 and transponders.

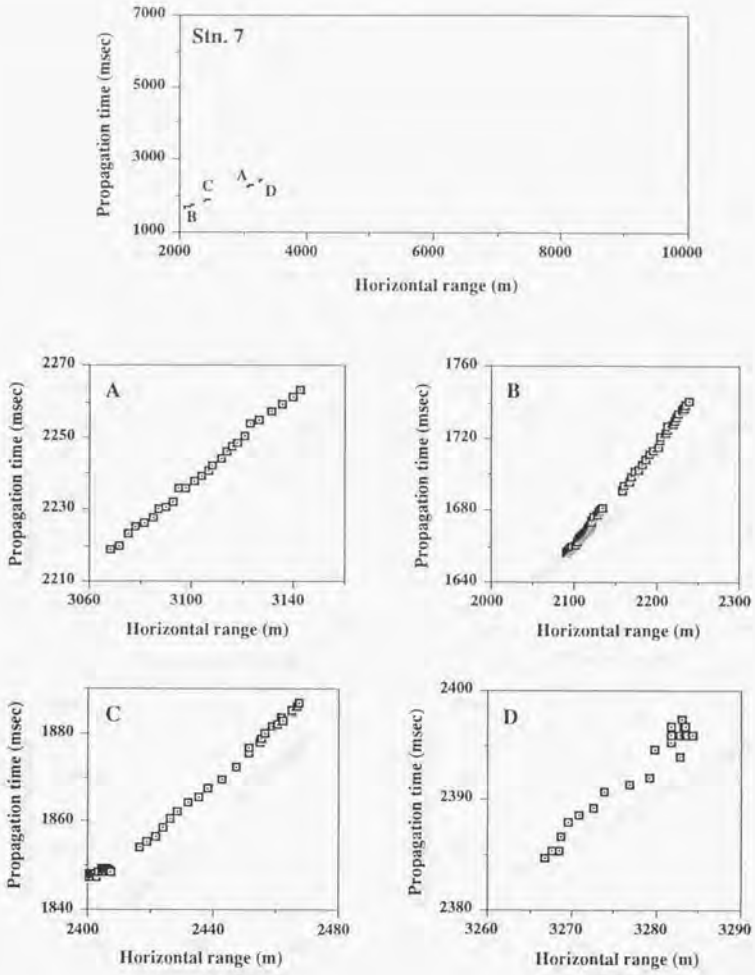

Figure 2-29 Propagation time from transponder A, B, C and D as a function of horizontal range between station 7 and transponders.

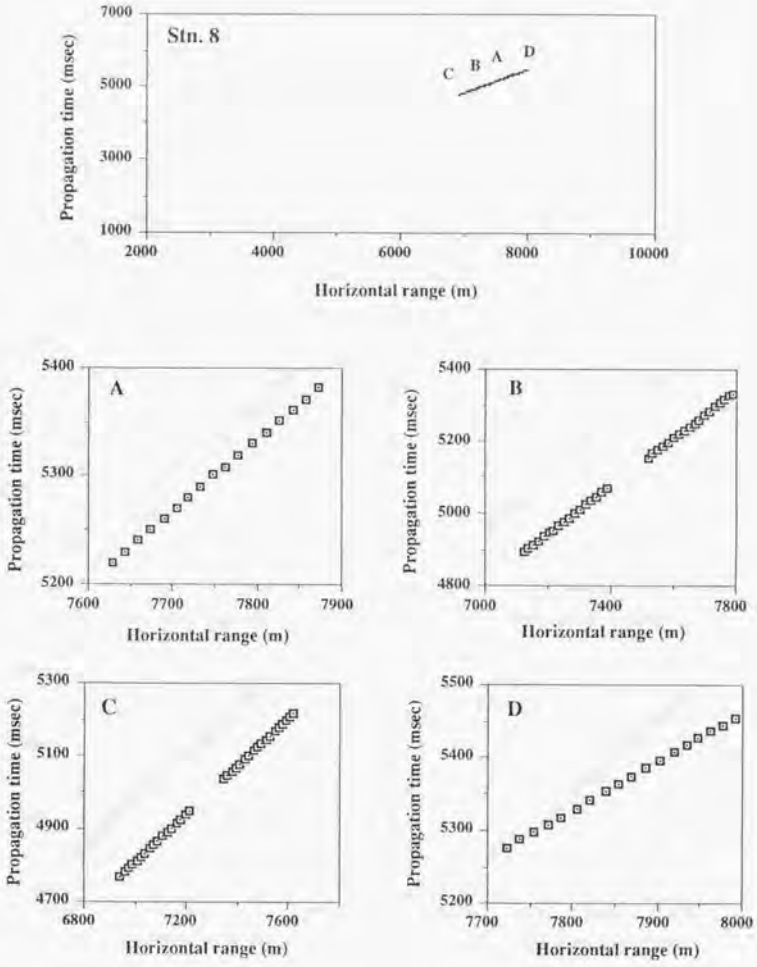

Figure 2-30 Propagation time from transponder A, B, C and D as a function of horizontal range between station 8 and transponders.

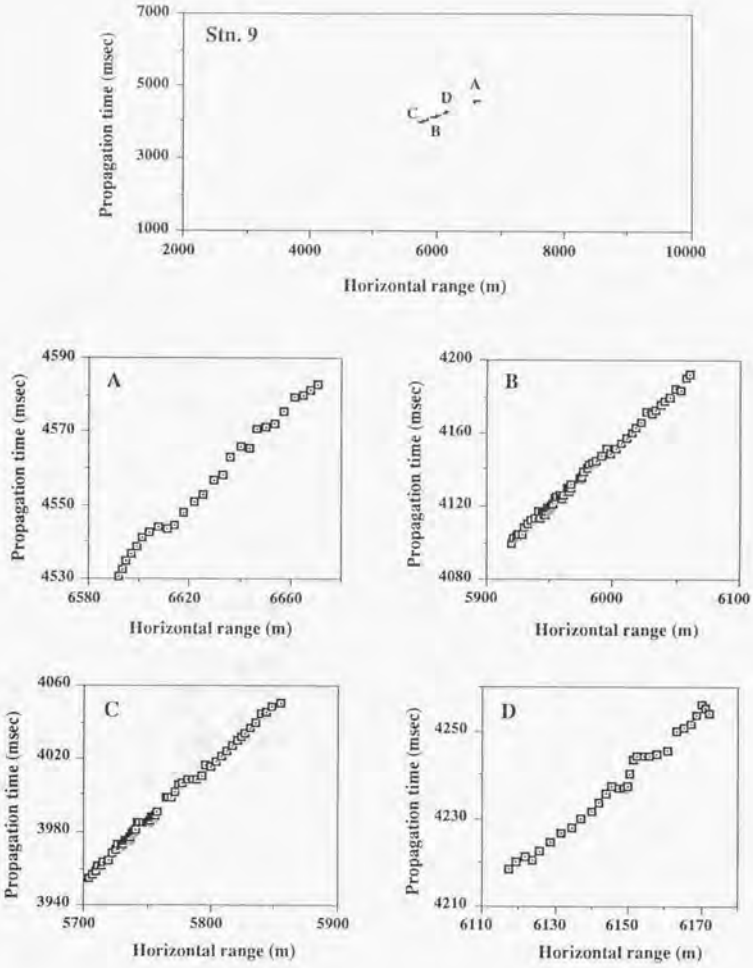

Figure 2-31 Propagation time from transponder A, B, C and D as a function of horizontal range between station 9 and transponders.

Table 2-3 Estimation error of sound speed(m/sec) and temperature(℃)(in parentheses) in relation to the number of data used and degree of Chebychev's polynomial.

		No. of Data								
		4	8	11	15	18	20	24	28	32
degree 2	Ave.	-0.34 (-0.08)	-0.29 (-0.10)	-0.29 (-0.10)						
	SD	1.65 (0,47)	1.41 (0.39)	1.41 (0.39)						
3	Ave.	-1.12 (-0.39)	-0.78 (-0.22)	-0.61 (-0.16)						
	SD	3.51 (0.98)	1.62 (0.37)	1.32 (0.36)						
4	Ave.		-0.75 (-0.21)	-0.63 (-0.18)						
	SD		1.42 (0.36)	1.09 (0.31)						
5	Ave.		-0.06 (-0.04)	0.10 (0.01)						
	SD		1.91 (0.47)	1.52 (0.38)						
6	Ave.		-0.64 (-0.18)	-0.42 (-0.14)						
	SD		1.04 (0.27)	1.40 (0.36)						
7	Ave.		-0.88 (-0.25)	-0.86 (-0.24)						
	SD		2.39 (0.59)	1.29 (0.34)						
8	Ave.			-0.94 (-0.27)						
	SD			1.12 (0.30)						
9	Ave.			-1.61 (-0.43)						
	SD			1.56 (0.40)						
10	Ave.			1.65 (0.88)	-0.85 (-0.24)	-0.18 (-0.08)	-0.62 (-0.18)	-0.70 (-0.19)	-0.67 (-0.19)	-0.63 (-0.19)
	SD			5.00 (1.90)	0.88 (0.25)	1.81 (0.47)	1.17 (0.31)	1.12 (0.29)	1.01 (0.29)	0.99 (0.26)

accuracy of sound speed(m/sec) and temperature(°C) expressed by the average and SD in relation to the number of data and the degree of the Chebychev's polynomials. The numbers of data and the degree of polynomial in the table correspond to Figures 2-33 and 2-34.

Figure 2-32 shows the arrangement of the stations and the transponders in this experiment and their combination used for sound speed estimation. The number of lines between the stations and the transponders correspond to the number of data used. Seven cases of combination with the number of data 32, 28, 24, 20, 18, 15 and 11 are shown. Using these data the variation of estimation accuracy with the number of data used was investigated, while the degree of the Chebychev's polynomial was fixed at 10.

Figure 2-33 shows the average and SD error of sound speed (upper) and temperature(lower) over the depth of 1400m from the surface to the bottom obtained from the estimation using ten degree Chebychev's polynomial. The horizontal axis is the number of data indicated in Figure 2-32. The average and the SD errors of sound speed/temperature are about -0.6m/sec / -0.2 °C and 1.0m/sec / 0.3 °C, when the number of data is larger than 15. Although the errors of the average values are likely to be negative, it is uncertain whether it is by a systematic error or not. From the result of Figure 2-33, it is found that the estimation accuracy is independent of the number of data when the degree of function is fixed. When the number of data is 11, however, the error jumped up largely as compared with the other case. This means that it is impossible to estimate 11 coefficients of the polynomial from 11 data with a high accuracy. When the data of propagation time involve unnegligible errors, it should be avoided to determine the coefficients by solving the simultaneous equations.

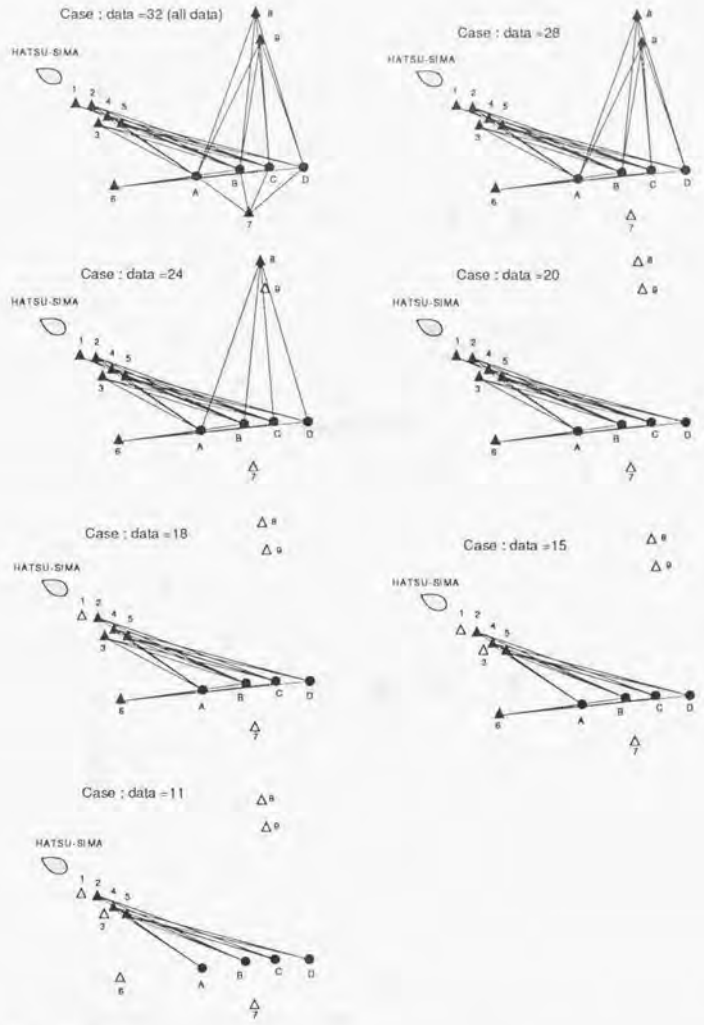

Figure 2-32

Combination of transponder(●) and station(▲) used for the estimation of sound speed and temperature using Chebychev's polynomial of 10degree. (△) : unused station.

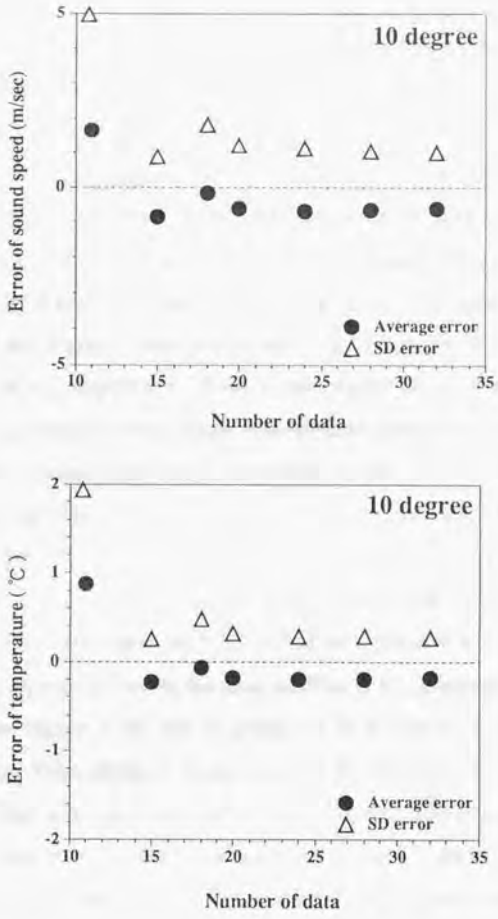

Figure 2-33

Dependency of error of sound speed(upper) and error of temperature(lower) in case of 10 degree Chebychev's polynomial on the number of data used for estimation.

In the next step, the variation of estimation accuracy with the degree of Chebychev's polynomial is described on condition that the number of data of propagation time is fixed. Figure 2-34 shows the arrangement of stations and the transponders used for the sound speed estimation(left) and the error of estimated sound speed as a function of degree of Chebychev's polynomial(right). Three cases of number of data (**a**):11, (**b**):8 and (**c**):4 are shown in the figure. The upper limitation of the degree of function in these cases becomes 10 in (**a**), 7 in (**b**) and 3 in (**c**), respectively. Even if the degree of polynomials is changed, no remarkable differences among three cases with repect to the estimation accuracy are seen except for the case of the maximum allowable degree. The total average and SD over three cases were -0.64m/sec(-0.17 °C) and 1.41m/sec(0.37 °C). Figure 2-35 shows the error profiles with depth of the sound speed(broken line) and the temperature(solid line) estimated using 2nd, 4th, 6th and 8th degree of Chebychev polynomials when the data number is 11 corresponding to the case (**a**) in Figure 2-34. The degradation of accuracy for the layer shallower than 200m depth is conspicuous in the case of the lower degree ,i.e., 2nd and 4th, compared with the case of higher degree. Figure 2-36 shows three profiles of sound speed(left): observed(solid dots), estimated by 2nd degree polynomial(solid line) and by 6th degree polynomial(dashed line) and two profiles of sound speed error(right) in case of 2nd and 6th degree polynomials. Figure 2-37 shows the temperature profiles(left) and temperature error profiles(right) that were converted from the sound speeds in Figure2-36. The errors of estimated sound speed throughout 1400m depth from the surface to the sea floor were -0.29m/sec in average and 1.41m/sec in SD for 2nd degree polynomial, and -0.42 m/sec in average and 1.40m/sec in SD for 6th degree. The difference in estimation error

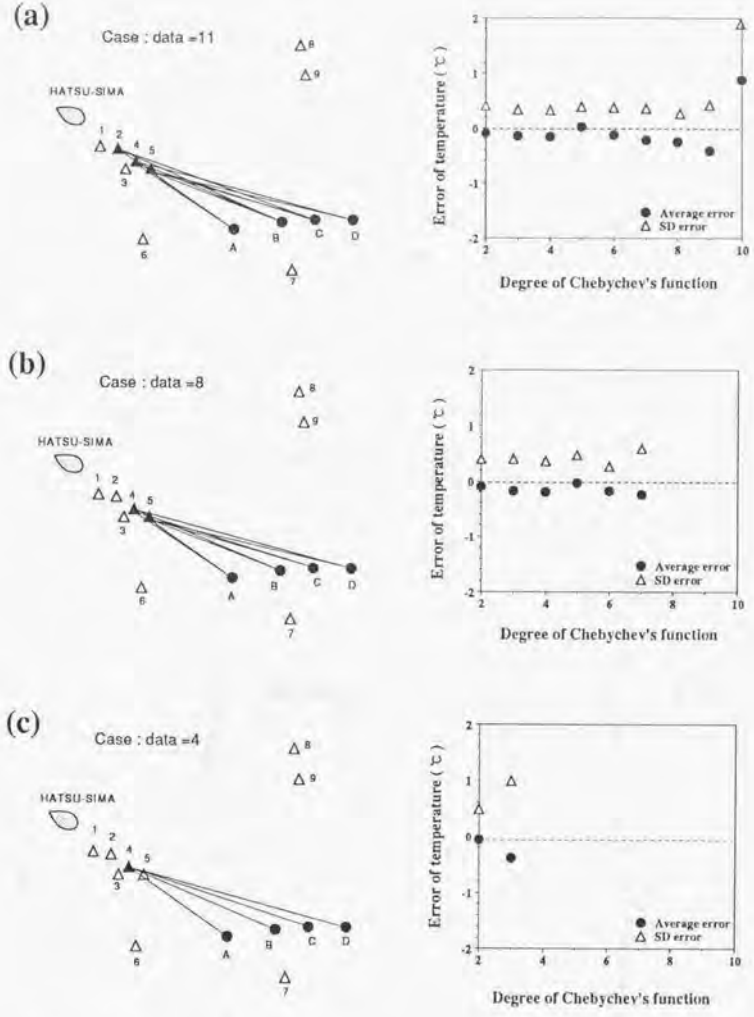

Figure 2-34

Data combination used for temperature estimation(left) and the estimation error of averaged temperature and standard deviation(SD)(right).
(a) Case : data = 11, (b) Case : data = 8, (c) Case : data = 4

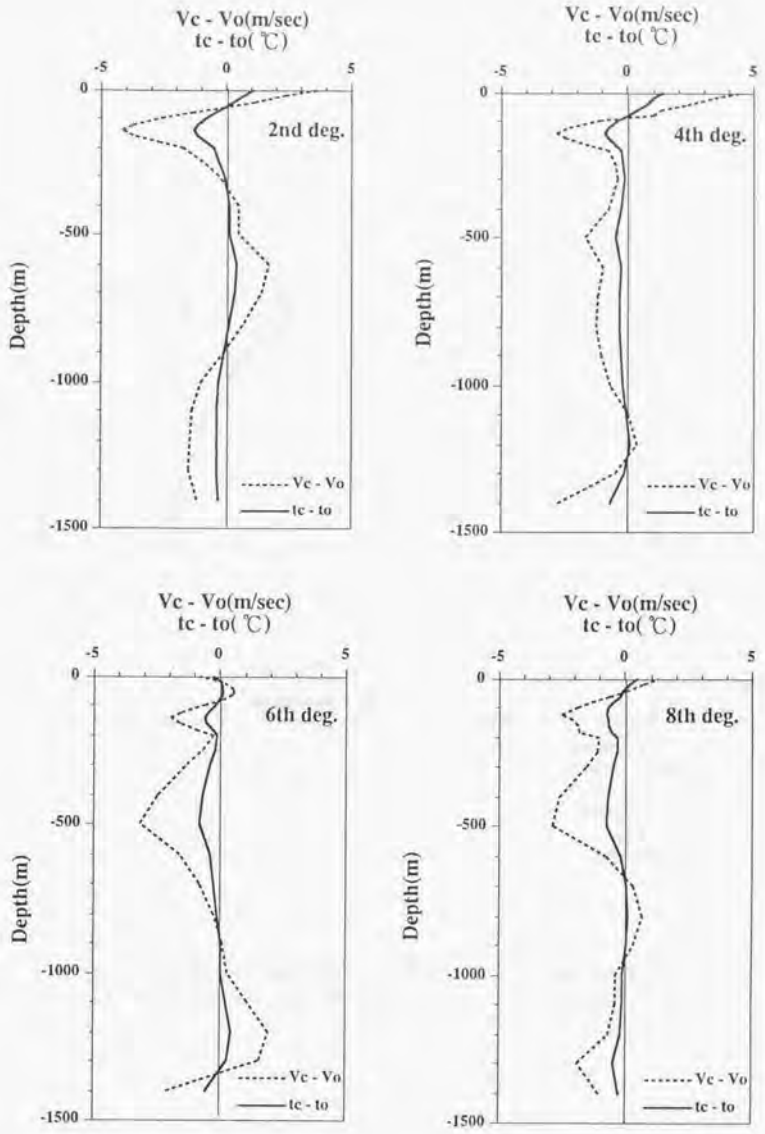

Figure 2-35 Estimation errors of sound speed and temperature in case of.2nd, 4th, 6th and 8th degree Chebychev polynomials.

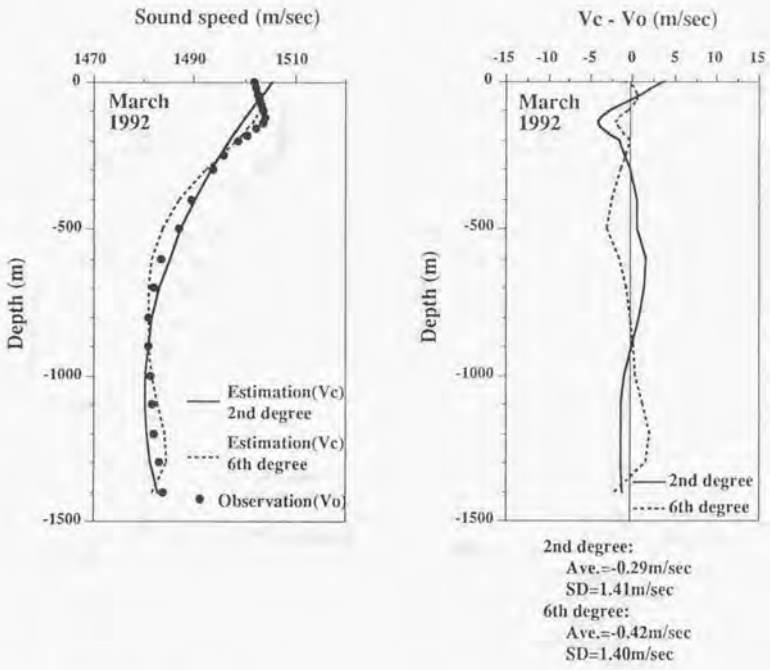

Figure 2-36

Comparison of sound speed profiles between observed and estimated by 2nd / 6th degree of Chebychev's function.

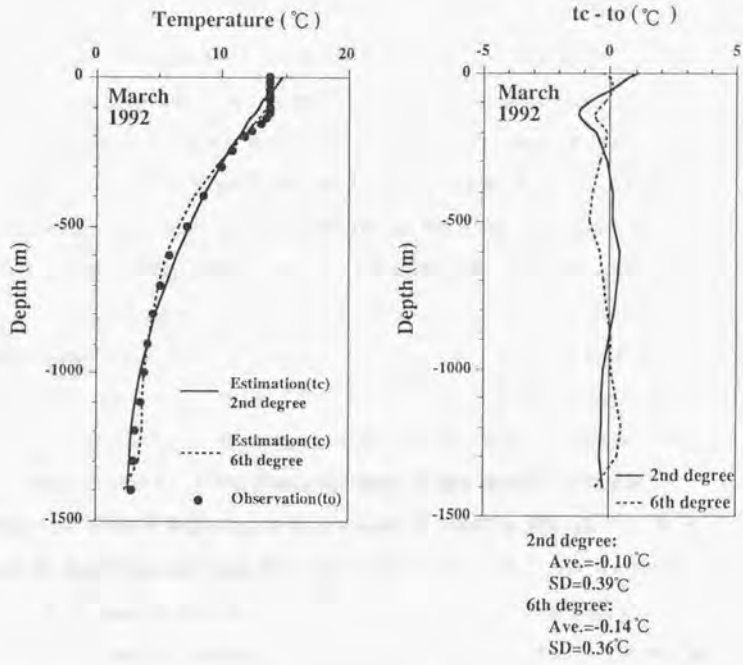

Figure 2-37 The temperature profiles(left) and temperature error profiles(right) that were converted from the sound speeds in Fig.2-36.

with the degree of polynomial appear more conspicuously in the layer shallower than 200m. For 2nd degree, the maximum difference is 7.84m/sec(max. is 3.67 m/sec at surface and min. is -4.17m/sec at 140m depth.). For 6th degree, the maximum difference is 2.45m/sec(max. is 0.52 m/sec at 40m depth and min. is -1.93m/sec at 140m depth). It is generally true that the higher the degree of polynomial used the better the estimation accuracy becomes.

Figure 2-38 shows, as a summary, the comparison between observed profiles(left) and estimated profiles(right) by 10th degree polynomial. The upper is sound speed and the lower temperature in cases of April(1991), May(1991) and March(1992) experiments.

The first thing to be mentioned about this result is that the temperature structures have been well estimated by the method of microtomographic technique. The second thing is that, however, the error of estimation seems to concentrate on the zone of shallow water, say, shallower than 200m. Since the error in the shallow water is improved when a high degree polynomial is used for the estimation, it may be recommended that the high degree polynomial, hence a large number of data, should be used for the estimation. But this idea involves an essential drawback, which contradicts our final objective to establish a simple system to enable us to monitor automatically and continuously the change of temperature structure of sea water. In other words it is necessary for us to develop another method which may improve the accuracy in the shallow water as well as reduce as much as possible the number of data required.

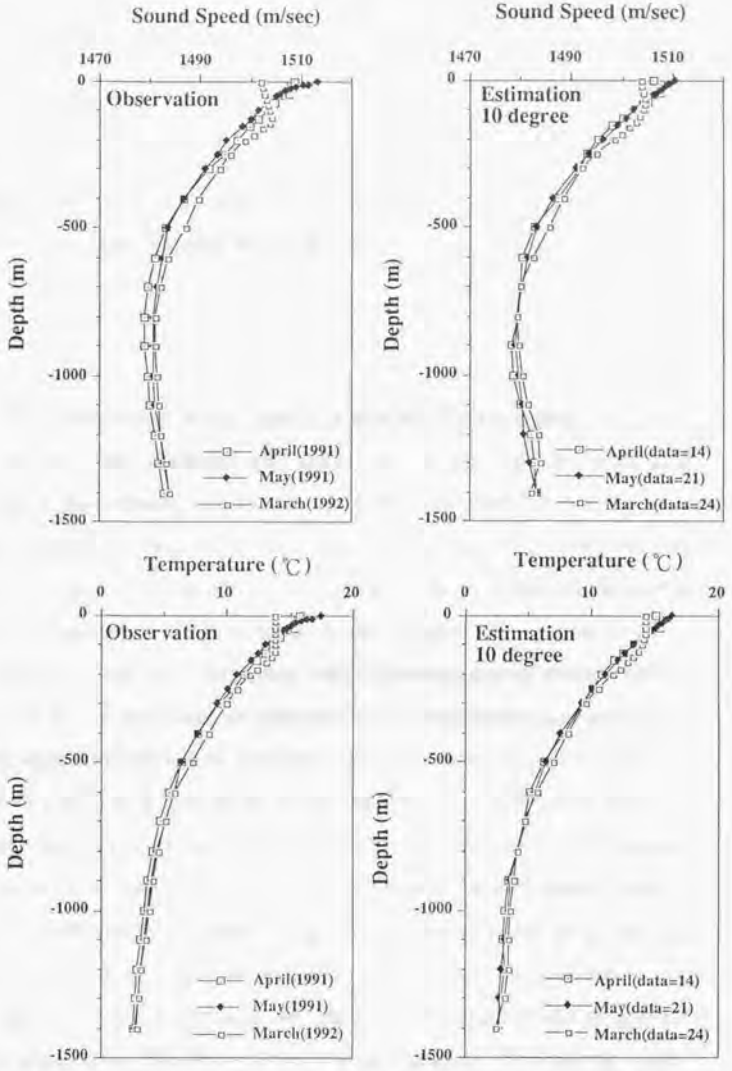

Figure 2-38 The comparison of profiles of the observed(left) and the estimated(right) by 10th degree polynomial. Sound speed(upper) and the temperature(lower) in cases of April(1991), May(1991) amd March(1992) experiments.

Chapter 3

3 Micro Tomographic Approach for the Shallow Sea

The knowledge of the vertical structure of sea temperature in the shallow sea is important not only to the coastal oceanography or fisheries but also to the regional oceanography which casts characteristic signals to the shallow water. When the low degree of Chebychev's polynomial was applied, as shown in Chapter 2, it was difficult to give the accurate sound speed profile for the shallow depth. In this chapter, the method to improve the accuracy is discussed with a few numbers of transponders.

There are two kinds of approach to understand the characteristics of sea water. The first is to measure a vertical mean of the physical properties such as temperature. As the temperature of water in the shallow layer shows a large variation due to the effects from atmosphere, inflow of fresh water from the river and the existence of thermocline, it is difficult to delineate faithfully the vertical change of temperature using the time of propagation of the acoustic signal. This is because the propagation time is essentially the result of integration of the parameters in the sound path. Therefore, if we change the mind of observing things, we will attain to an idea of making direct use of the nature of the acoustic signal propagation. The propagation time is directly connected to the vertical mean of water temperature(and salinity and pressure), so it may be possible to relate the propagation time of acoustic signal with the mean

physical parameter in a certain layer, which is significant from the oceanographic point of view.

The second is to apply the inversion method to the acoustic propagation time data as we conducted in the experiments described in the previous chapters. As for the shallow sea, however, the observations and the inversion have to be made in double steps, i.e., additional transponders are installed at the shallow bottom to conduct microtomography within a shallow layer. In this chapter the two methods and their applications are described through simulation using the data available at present.

3.1 Application of Mean Temperature Estimation Method to the Shallow Sea

Rossby(1969) showed that the vertical round-trip propagation time monitored by the Inverted Echo Sounder(IES) is effective as an index of thermocline depth. This means that the round-trip time depends on the ratio of warm water to cold water, i.e., the depth of the thermocline. Watts and Rossby(1977) also pointed out that the propagation time data measured by IES becomes a good index of the dynamic height, and this was confirmed from the observation in the eastern Pacific by Chiswell(1986). The IES is regarded as an acoustic monitoring system which offers the integrated information of vertical sea temperature distribution.

If the mean temperature in the shallow sea is estimated from a propagation time data between a pair of transponders, it will become a good index to monitor the variability of vertical sea temperature distribution.

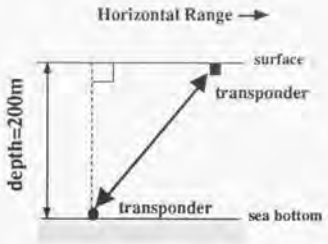

Figure 3-1 Configuration of a pair of transponder for the estimation of mean temperature.

In this section, by assuming a system consisting of two transponders installed at surface and bottom in a shallow water, we attempted to formulate a regression line which represents the relationship between the vertical mean temperature and the propagation time of acoustic signal. The data used to demonstrate the plausibility of our approach are those supplied from the Kanagawa Prefectural Fisheries Experimental Station.

It is reported by many authors(Iwata and Matsuyama,1989; Kawabe,1985,1986; Matsuyama and Iwata,1977; Taira and Teramoto,1986) that the flow, the sea level and the water properties in the Sagami Bay are closely related to the variation of path of the Kuroshio current. The Kuroshio has three quasi-steady paths, i.e., the nearshore and the offshore non-large-meander paths(nNLM and oNLM) and the typical large-meander path(tLM). If the temperature anomalies in the Sagami Bay is assumed zero for nNLM path, then they become positive for tLM path and negative for oNLM path(Kawabe and Yoneno,1986). We must pay attention to the phenomena that the difference of sea temperature around the bay between tLM and oNLM path periods becomes large, because our analysis was made in such periods.

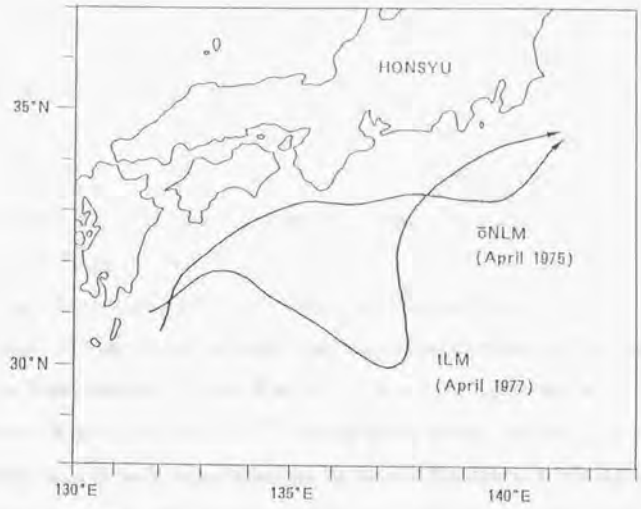

Figure 3-2 The Kuroshio paths of tLM in April, 1977 and oNLM in April, 1975.

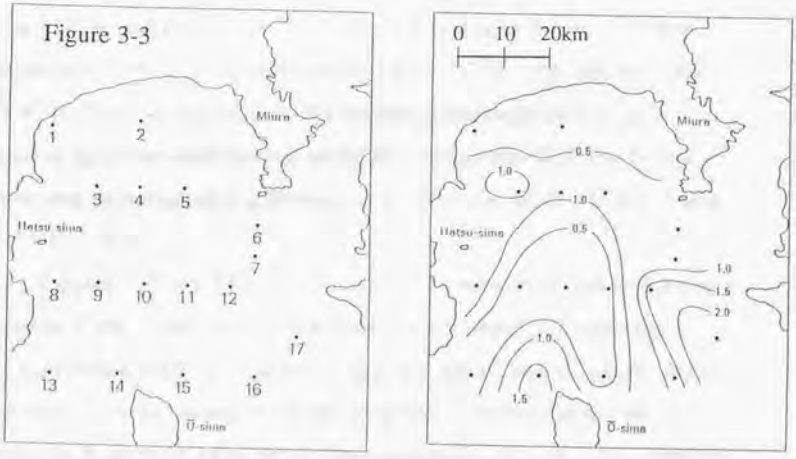

Figure 3-4 The contour map of the differences of mean temperature with 0.5 °C interval between tLM and oNLM(tLM - oNLM). The contour was drawn using the temperature data observed at the stations shown in Figure 3-3.

Figure 3-2 shows the Kuroshio paths of tLM in April, 1977 and oNLM in April, 1975(Kawabe,1985). From this figure, it is found that the path during tLM approaches the Sagami Bay after the large meander off the Ensyu Nada. The path during oNLM takes relatively an offshore course of the Sagami Bay.

The temperature and salinity data in the Sagami Bay used were those observed monthly at the fixed stations by the Kanagawa Prefectural Fisheries Experimental Station. Figure 3-3 shows the locations of observation stations(No.1 ~ No.17) used in this analysis. Table 3-1 shows the temperature at each layer from the surface to the 200m depth and the mean value in April, 1975 for the case of (oNLM) and in April, 1977 for the case of (tLM). The mean temperature in tLM period is higher than in oNLM period all over the stations. The total average temperature is 12.75 °C in oNLM and 13.59 °C in tLM. The contour of difference of mean temperature between tLM and oNLM(tLM - oNLM) with the interval of 0.5 °C is shown in Figure 3-4. The tendency of temperature high is outstanding at the southern part of the bay around the O-Shima Island. There was no remarkable difference as to the mean salinity in both paths of the Kuroshio.

Figures 3-5 and 3-6 show the mean temperature(t_m) in degrees as a function of the sound propagation time(T) in msec(right) when the horizontal range(HR) is 0km (vertical propagation) and 1km(left), 2km and 3km. Acoustic transponders are assumed to be fixed at the surface and at the bottom of 200m depth. The propagation time was calculated by using the temperature shown in Table 3-1 and the salinity data observed in the same periods. Although the groups of points for oNLM case and tLM case are separated in the figure, t_m data of both groups align on a straight line. A regression line $t_m = \alpha + \beta T$ derived from both data are

Table 3-1 The temperature at each layer from the surface to the 200m depth and the mean temperature in April, 1975(oNLM) and in April, 1977(tLM) reported by the Kanagawa Prefectural Fisheries Experimental Station.

April 1975(oNLM)

Depth	Station																
	1	2	3	4	5	6	7	8	9	10	11	12	13	14	15	16	17
0	14.3	14.8	15.0	15.0	14.7	13.4	13.5	13.7	14.3	14.6	14.5	13.7	14.3	14.0	14.6	14.1	13.6
10	14.1	14.6	14.6	14.40	14.54	12.99	13.10	13.68	14.19	14.47	14.11	13.39	14.13	13.90	14.51	13.49	13.32
20	13.89	14.2	14.4	13.96	14.21	12.95	13.23	13.69	14.12	14.38	14.11	13.57	14.14	13.82	14.42	13.58	13.31
30	13.87	14.0	14.14	13.98	14.07	12.91	13.60	13.76	14.12	14.40	14.09	13.60	14.09	13.77	14.36	13.59	13.36
50	13.86	13.9	13.88	13.75	14.04	13.46	13.77	13.71	14.08	14.32	14.09	13.82	14.07	13.79	14.33	13.69	13.06
75	13.47	13.67	12.99	13.22	13.61	12.58	13.81	13.68	14.00	14.10	14.06	13.77	13.75	13.76	13.81	13.85	12.52
100	12.61	13.10	12.42	12.64	13.03	13.09	13.11	13.06	13.43	13.25	13.85	13.05	13.09	13.67	13.03	12.68	12.2
150	11.24	11.80	11.47	11.42	11.93	11.29	11.17	11.88	12.54	12.47	12.40	11.71	11.63	12.35	12.24	11.55	11.13
200	10.36	10.67	10.49	10.34	10.73	10.41	10.65	10.68	11.28	11.45	10.99	10.66	10.78	11.66	11.57	10.97	10.88
mean	12.47	12.85	12.65	12.63	12.89	12.33	12.44	12.61	13.13	13.22	13.17	12.59	12.77	13.09	13.15	12.60	12.18

April 1977(tLM)

Depth	Station																
	1	2	3	4	5	6	7	8	9	10	11	12	13	14	15	16	17
0	14.2	14.8	15.4	15.9	14.3	14.9	15.1	14.5	15.3	16.0	16.4	17.0	15.5	17.5	15.2	16.5	16.0
10	14.6	14.7	15.1	15.53	14.73	14.80	14.97	14.55	15.0	16.06	15.76	16.50	15.49	17.74	14.88	15.68	15.67
20	14.47	14.5	14.81	15.3	14.49	14.80	14.90	14.51	14.90	15.76	15.64	15.90	15.27	17.73	14.78	15.64	15.25
30	14.42	14.5	14.74	14.94	14.47	14.80	15.01	14.62	14.80	15.52	15.59	15.40	15.13	17.49	14.80	15.63	15.28
50	14.45	14.28	14.51	14.09	14.52	14.60	14.57	14.43	14.60	15.23	14.69	15.00	14.19	16.09	14.65	14.32	15.02
75	13.76	13.97	13.65	13.71	14.49	13.10	13.76	14.25	13.50	14.67	13.84	14.30	13.78	15.52	14.62	13.96	14.83
100	13.25	13.39	13.10	13.34	14.26	12.80	12.95	14.07	13.40	13.37	13.75	13.90	13.39	15.01	14.54	13.68	14.73
150	11.62	12.08	13.34	12.01	13.00	12.10	12.06	12.70	12.40	12.07	12.30	13.00	12.38	13.2	12.22	13.10	14.20
200	10.69	10.89	11.43	11.34	11.76	11.50	11.05	10.88	11.00	11.36	11.12	11.90	10.68	11.74	11.26	12.25	12.72
mean	12.84	13.09	13.76	13.34	13.57	13.18	13.15	13.32	13.34	13.61	13.65	14.16	13.23	14.72	13.57	13.97	14.53

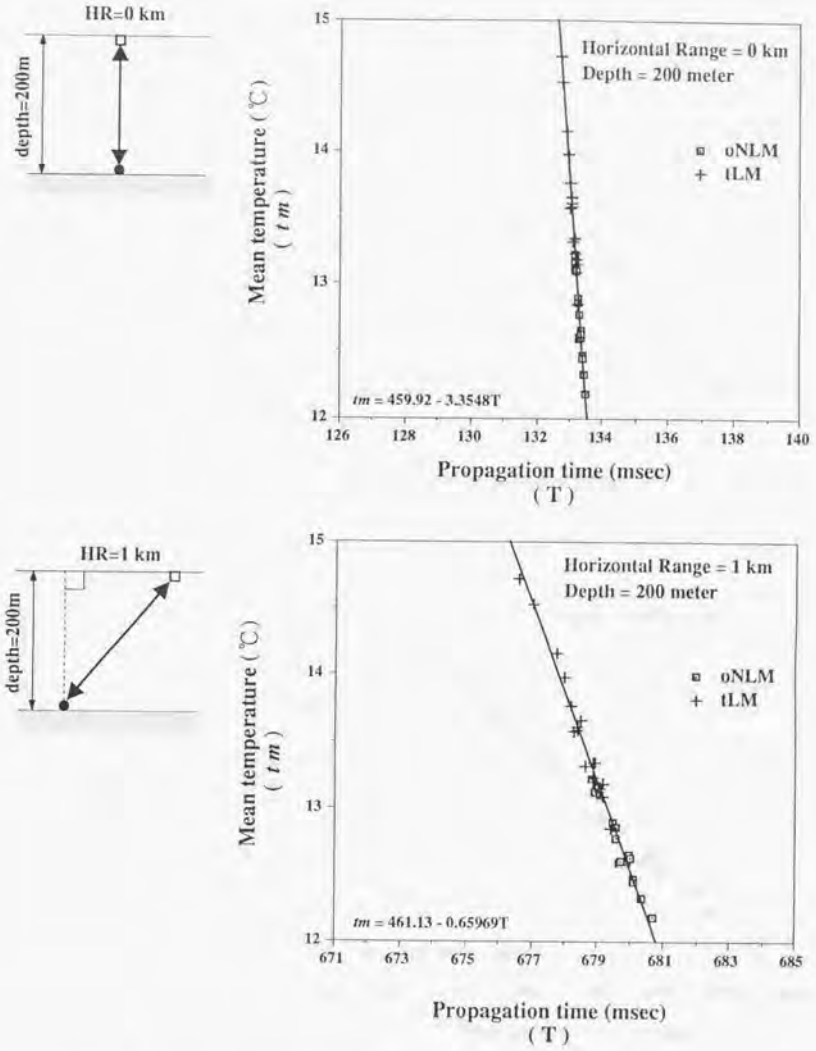

Figure 3-5 The mean temperature(*tm*) in degree C as a function of the sound propagation time(T) in msec(right) in horizontal range(HR) cases of 0km(vertical propagation) and 1km(left).

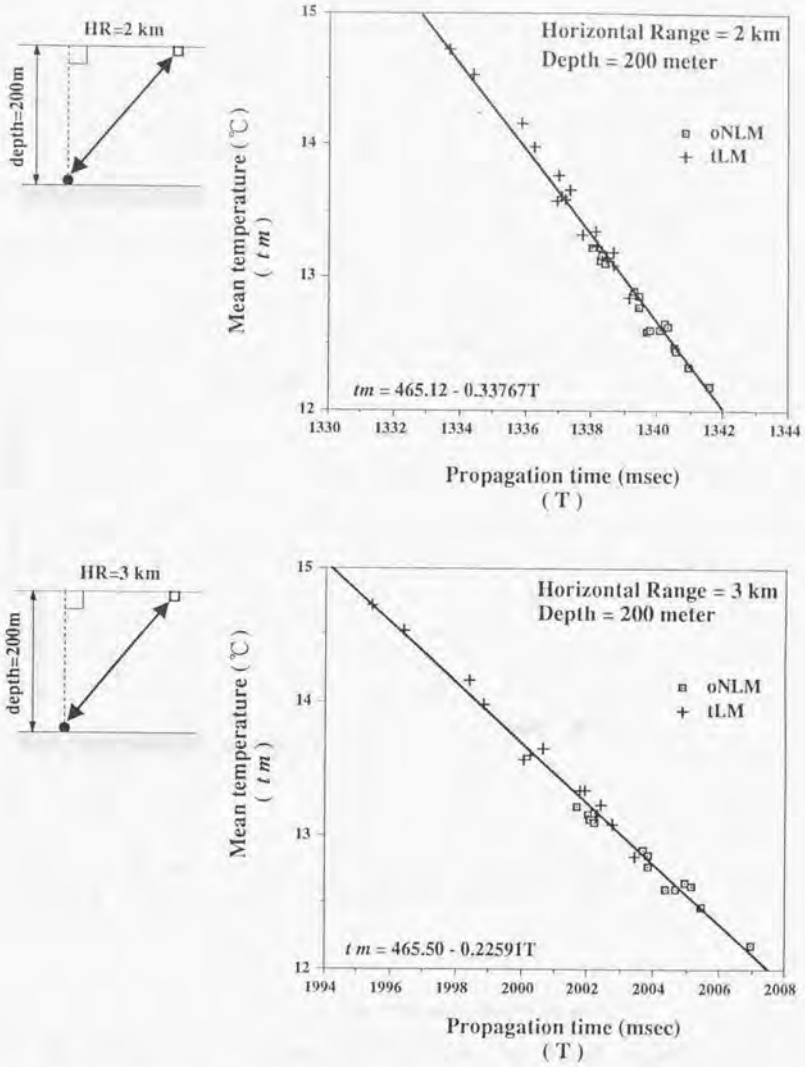

Figure 3-6 The mean temperature(tm) in degree C as a function of the sound propagation time(T) in msec(right) in horizontal range(HR) cases of 0km(vertical propagation) and 1km(left).

plotted in each figure. α and β are coefficients, T is propagation time in msec and t_m temperature in °C.

Figure 3-7 shows the gradient(this corresponds to β) of mean temperature for propagation time as a function of the horizontal range. The values of β are indicated in the regression lines in Figure3-5 and 3-6.

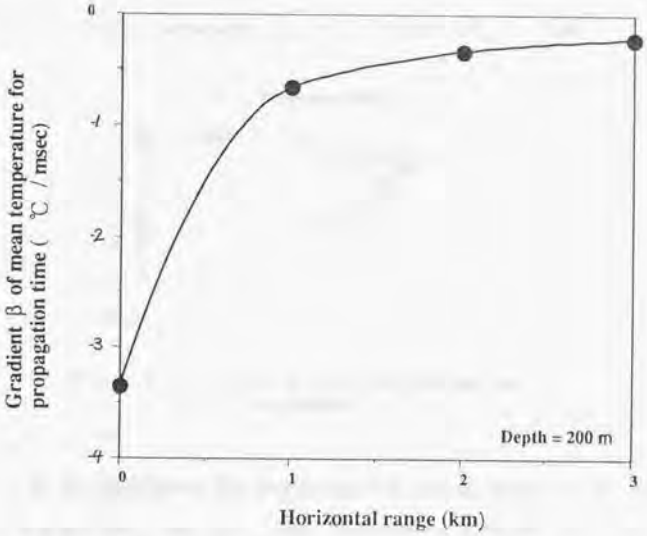

Figure 3-7 The gadient(β) of mean temperature against the propagation time as a function of the horizontal range.

The gradient β in °C/msec approaches zero with the increase of horizontal range. Although β is -3.35 °C/msec for horizontal range=0, β decreases to -0.23 °C/msec for horizontal range of 3km. This means that the longer the horizontal range is, the higher the accuracy of mean temperature becomes provided the time measuring accuracy is the same. Thus, we knows that it is easy to evaluate a mean temperature from the propagation time between two transponders.

3.2 Application of Microtomographic Method to the Shallow Sea

The estimation accuracy of sound speed profile for 200m and 500m depth is discussed by simulation approach. Four propagation time data as used for the microtomographic inversion method mentioned in Chapter 1 are also assumed to be provided by combining a transponder at the sea surface and four transponders at the sea bottom(Figure 3-8).

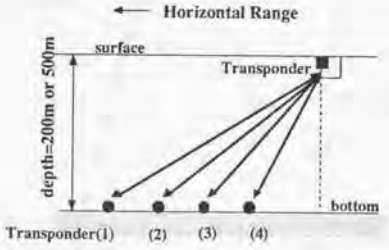

Figure 3-8 Configuration of transponders for estimation of sound speed profile.

In the simulation, the sound speed profile of March, 1992, was used as an observation. The 2nd degree Chebychev polynomial was employed for the estimation. This means that three coefficients of 2nd degree Chebychev polynomial are estimated from four propagation time data by inversion. The horizontal range between the transponder at the surface and the nearest transponder(4) at the bottom in Figure3-8 is 1km and the separation of transponders at the bottom is 0.5km. The errors in the time measurement generated from the normal random probability distribution $N(0, \sigma^2)$ were added artificially to the calculated propagation time data based on the actual sound speed profile. The sound speed thus estimated is converted to the sea temperature.

Figure 3-9 shows the observed(March, 1992) and estimated temperature profiles to 500m depth(left), and the temperature estimation error profile(right).

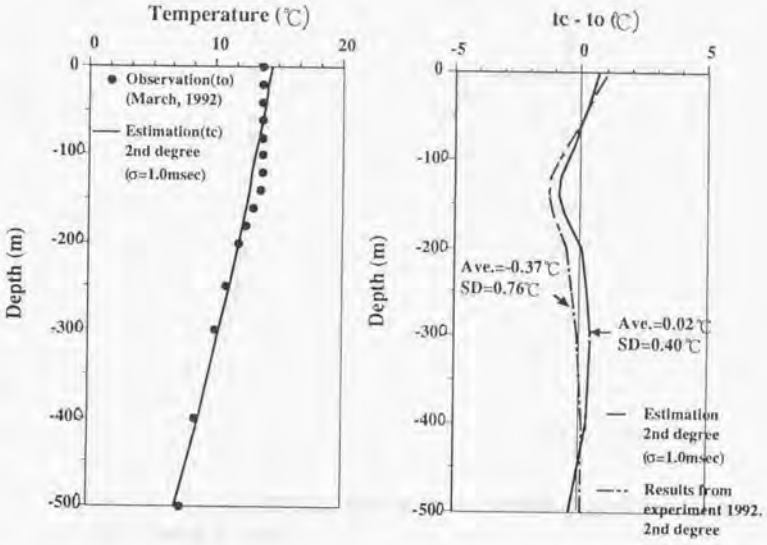

Figure 3-9 The observed and estimated temperature profiles to 500m depth(left), and the profiles of estimation error of temperature(right).

The error of propagation time for σ =1msec was given in this case as in the case of the experiment (I) and (II) in the Sagami Bay. The profile(broken line) in the right figure is a portion of temperature estimation error by 2nd degree Chebychev polynomial, which is extracted from the result of experiment 1992. This is added to the figure for comparison.

The estimation errors was -0.37 °C in average and 0.76 °C in SD in the experiment 1992. On the other hand the error became -0.02 °C in

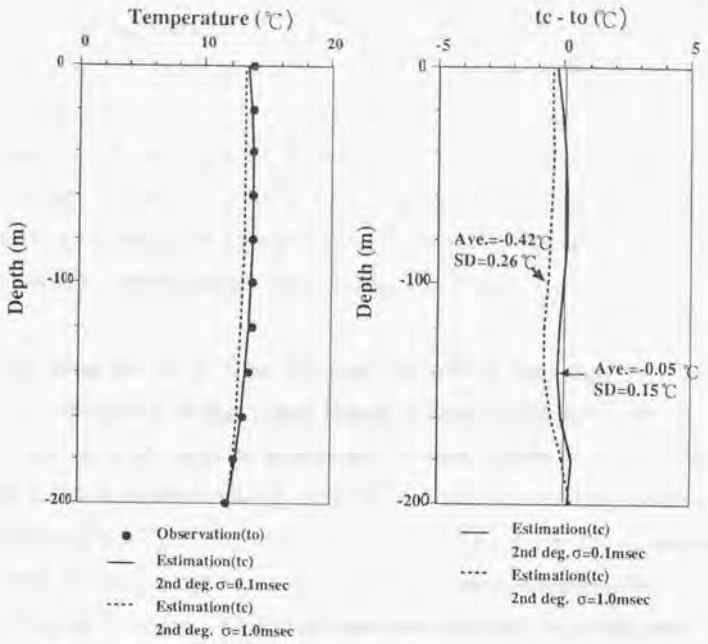

Figure 3-10 The temperature profiles down to 200m depth(left) and the error profiles(right).

average and 0.40 °C in SD in this simulation. Although the maximam error of 0.9 °C is seen at 130m depth, a remarkable improvement in accuracy is seen as a whole. When the number of tansponders are the same, a higher estimation accuracy than otherwise can be attained by installing the transponders at the shallow depth.

Figure 3-10 shows the temperature profiles to 200m depth(left) and the error profiles(right). In the figures, the profiles of observation in March, 1992(solid circle in the left figure) and estimation by 2nd degree Chebychev polynomial are shown. In this case σ has been changed: the error σ =0.1msec(solid line) and σ =1.0msec(broken line) are adopted. The result shows that the estimation errors in case σ =0.1msec were -0.05

°C in average and 0.15 °C in SD, whereas the errors in case σ =1.0msec were -0.42 °C and 0.26 °C, respectively. It is found from this result that to reduce the error of measurement of propagation time is very important for the better estimation accuracy. The time measurement accuracy of 0.1msec is not so difficult to attain by the current ocean acoustic technique that the precise estimation of temperature profile will be at hand by the acoustic tomographic approach.

3.3 Proposal of a Total System for Microtomography

In order to design a total system of microtomography, the following points must be considered: (1) Performance of the transponder as for the transmission level, receiving sensitivity and the frequency of sound signal. (2) Topography of sea floor and the depth. (3) Receivable range of direct propagation wave. (4) The minimum number of transponder required to get high estimation accuracy of sound speed structure. In this section, we would like to propose a fixed system which does not require an oceanographic vessel.

Figure 3-11 shows an arrangement of transponders proposed for the microtomographic monitoring system(upper) and the section along the line **L** in the upper figure(lower). This acoustic network is supposed to be located off the eastern part of the Hatsu-Shima Island where our experiments were carried out. By this network a section of mean structure of sound speed on the line **L** will be estimated continuously. The system consists of a control transponder set(CT) at the near sea surface and five transponders T1,T2,T3,T4 and T5 for the deep sea tomography and Ta, Tb, Tc and T1 for the shallow sea tomography. These are installed on the sea floor. The horizontal range between T1 and T5 is 6km. The distance 6km corresponds to the maximun receivable range in summer season. In order to get maximum performance with the

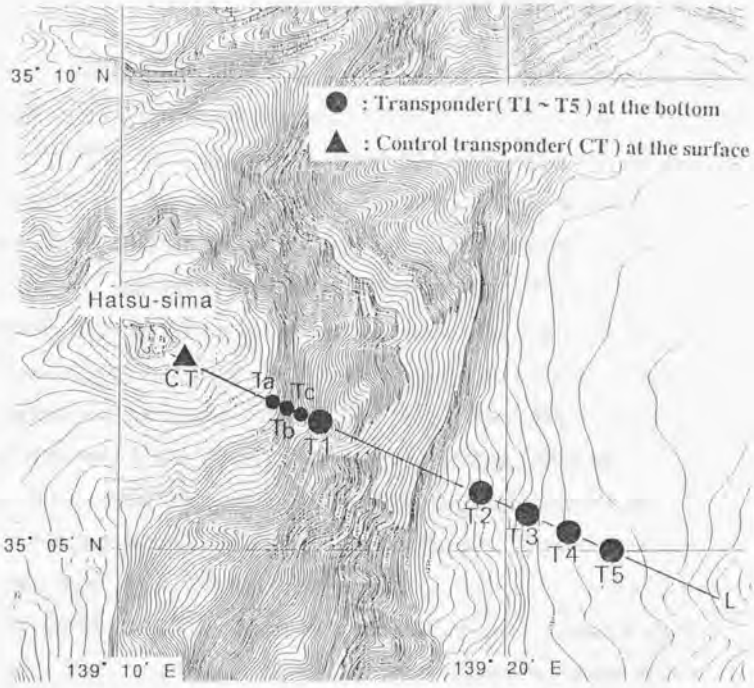

Sectional plan at line **L** in upper figure

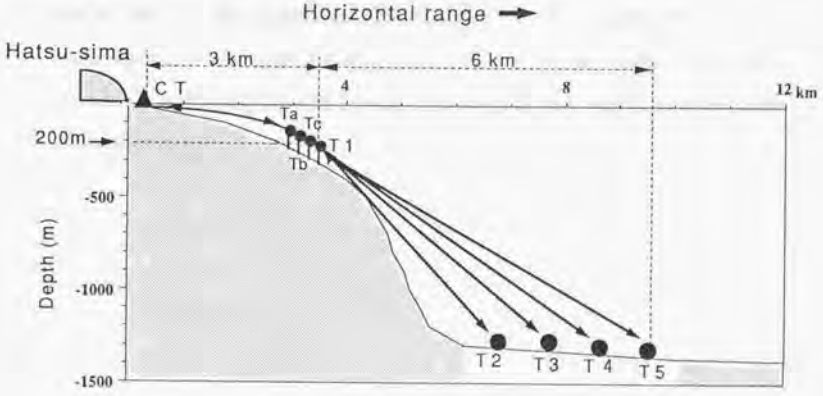

Figure 3-11 A configuration of transponders proposed for the microtomographic monitoring sytem(upper) and the sectional plan at line **L** in upper figure(lower).

minimum number of transponders, the number of transponders is selected to be five. The four data of propagation time from T2,T3,T4 and T5 are transferred to the land station on the Hatsu-Shima Island acoustically by T1 through CT. The raw propagation time data are processed there to determine the structure of sound speed in the layer deeper than 200m and recorded. The 2nd degree Chebychev polynomial is used for the estimation of the areal mean sound speed profile. The round trip propagation time between CT and T1 is monitored continuously to check the variation of mean temperature in the shallow layer. The horizontal range between CT and T1 is 3km. In order to conduct a high accuracy estimation of mean temperature by use of the slantingly propagating signal, transponders CT, T1, Ta, Tb and Tc are used. The depths of T1, Ta, Tb, Tc are about 200m and four propagation time data between CT and T1~Tc are used. The estimation in the shallow layer is made using a similar inversion method employing 2nd degree Chebychev polynomial as in the case of the deep sea.

Although the use of two systems for the deep sea and the shallow sea is proposed here, the microtomography itself is possible by either of the system. In any case the best configuration of transponders must be decided considering the sea bottom topography and depth at the sea area to be monitored.

Chapter 4

4 Conclusion

The ocean acoustic microtomographic technique was developed, by which the areal mean of vertical sound speed or temperature in a few kilometer area is estimated from the propagation time of the acoustic signal between a sound source at the sea bottom and a receiver at the sea surface.

In the age of 200 mile economical zone when the importance of offshore or coastal fishing is advocated, the three dimensional, long term and continuous monitoring system for the fisheries and oceanography in the fishing ground is more and more needed. And the idea of the tomographic approach has a possibility of application to the oceanographical remote sensing in investigating the focused sea area such as the Kuroshio/Oyashio current area or the water frontal area and so on.

From the verification experiment in the Sagami Bay of 1991 and 1992, the sea temperature with the accuracy 0.2~0.3 ^{o}C could be estimated by the inversion method using the Chebychev polynomial over the depth of 1400m. Although the estimation error was large comparatively in the layer shallower than 200m, the estimation accuracy is expected to be improved by adding transponders in the shallow water. Judging from these results, the microtomographic approach in which the directly propagating acoustic signal is used positively has being proved to be effective as a remote sensing technique for the monitoring of oceanic

variability in the small scale. It was also shown that the propagation time of acoustic signal between a pair of transponders at the sea surface and the sea floor will become a good indication of the variation of mean temperature in the shallow layer. Taking these results into cosideration, a total system for microtomography was discussed by proposing the development of a system in the Sagami Bay as the first challenge.

The quality of oceanic information will be raised by microtomographic data combined with the surface temperature image of artificial satellite and the hydrographic observations. Although an initial investment will be needed for the acoustic tomography to be achieved, it should turn out to be rather economical if the merits of long term, continuous and real time monitoring are considered.

Some tasks remain in the actual operation of microtomogaphy system. In order to realize a higher estimation accuracy of sound speed structure, the measurement of more precise propagation time is needed. For example, if the resolution accuracy of mean temperature higher than 0.1 ^{o}C is aimed at, the time measurement accuracy higher than 0.1msec would be required. The accuracy of synchronization between the clocks of the source and receiver, the improvement of S/N ratio by employing M sequence signal or the phase measuring technique of compressed pulse transmission remain as the future tasks on the time measurement. The geometrical relation between the locations of the source and the receivers and the positioning accuracy , and the number of receivers available are also important in practical use. The use of the bottom stations installed on the sea floor in the Sagami Bay by Fujimoto et al.(1988), and the monitoring of relative location by the Long Baseline positioning developed by Fujimoto et al.(1988) may give an answer for the location problem.

Although a new idea of inversion method must be figured out for the three dimensional analysis, it may be solved by devising a proper method of deploying multiple transponders in the three dimensional scale. Our important tasks would be, thus, the total design of microtomography system, the establishment of maintenance method and the installation/recovery techniques for practical use.

References

Chiswell S., D. Watts and M. Wimbush : Using Inverted Echo Sounders to Measure Dynamic Height in the Eastern Equatoial Pacific During the 1982-1983 EL Nino, Deep Sea Res., **33**:981-991. (1986).

Clay M. : Acoustical Oceanography, John Wiley & Sons, New York. pp86.

Cornuelle B., C. Wunsch, D. Behringer, T. Birdsal, R. Heinmiller, R. Knox, K. Metzger, W. Munk, J. Spiesberger, R. Spindel, D. Webb and P. Worcester : Tomographic Maps of the Ocean Mesoscale, Part I:Pure Acoustic, J. Phys. Oceanogr., **15**:133-152. (1985).

Farmer D.M. and Lemon D.D. : The Influence of Bubbles on Ambient Noise in the Ocean at High Wind Speeds, J. Phys. Oceanogr., **14**:1762-1778. (1984)

Fujimoto H., J. Segawa and T. Furuta : Installation of Ocean Bottom Observation Station by Means of Underwater Acoustic Positioning, Zisin, **41**:583-589. (1988). (in Japanese)

Fujimoto H., T. Furuta and H. Murakami : Underwater Positioning by Long-Baseline Acoustic Navigation System and Relocation of Transponders, Marine Geodesy, **12**:201-219. (1988).

Furuta T., H. Fujimoto, Y. Tomoda, K. Kobayasi and H. Murakami : A Handy Acoustic Transponder Navigation System, Development and Operation, J. Geod. Soc. Japan, **30**:313-322. (1984).

Iwata S. and M. Matsuyama : Surface Circulation in Sagami Bay: the Responce to Variations of the Kuroshio Axis, J. Oceanogr. Soc. Japan, **45**:310-320. (1989).

Japan Hydrographic Association : Study on the Investigation method of Ocean structure by Acoustics, Report No.**52** 1-160. (1989). (in Japanese)

Kakihara T. and J. Segawa : Feasibility of the Ocean Acoustic Micro Tomography, J. Tokyo Univ. Fish., **78**(1):45-55. (1991).

Kakihara T. and J. Segawa : Discussion on the Positioning of Sound Source in the Ocean Acoustic Micro Tomography, J. Tokyo Univ. Fish., **78**(2):179-186. (1991).

Kakihara T. and J. Segawa : The Ocean Acoustic Micro Tomography for the Case of the Sagami Bay Model, J. Tokyo Univ. Fish., **79**(1):95-101. (1992).

Kawabe M. : Sea Level Variations at the Izu Islands and Typical Stable Path of the Kuroshio, J. Oceanogr. Soc. Japan, **41**:307-326. (1986).

Kawabe M. : Study on the Kuroshio and Tsusima Current: Variation of the Current Path, J. Oceanogr. Soc. Japan, **42**:319-331. (1986).

Kawabe M. and M. Yoneno : Water and Flow Variations in Sagami Bay under the Influence of the Kuroshio Path, J. Oceanogr. Soc. Japan, **43**:283-294. (1987).

Knudsen V.O., R.S. Alford and J.W. Emling : Underwater Ambient Noise, J. Mar. Res., **7**:410-429. (1948).

Lemon D.D., D.M. Farmer and D.R. Watts : Acoustic Measurement of Wind Speed and Precipitation over a Continental Shelf, J. Geophys. Res., **89**:3462-3472. (1984).

Leroy C.C. : Development of Simple Equations for Accurate and More Realistic Calculation of the Speed of Sound in Sea Water, J. Acoust. Soc. Am., **46**:216-226. (1969).

Mackenzie K.V. : Nine-Term Equation for Sound Speed in the Oceans, J. Acoust. Soc. Am., **79**:807-812. (1981).

The Marine Acoustic Society of Japan : Report of the Tomography Session, No.**12** 1-176. (1986). (in Japanese)

Matsuyama M. and S. Iwata : The Kyucho in Sagami Bay, Bul. Japanese Soc. Fish. Oceanogr., **30**:1-7. (1977). (in Japanese)

Munk W.H. : Sound Channel in an Exponentially Stratified Ocean with Application to SOFAR, J. Acoust. Soc. Am., **55**:220-226. (1974).

Munk W.H. and A. Forbes : Global Ocean Warming, An Acoustic Measurement, J. Phys. Oceanogr., **19**:1765-1778. (1989).

The Ocean Tomography Group : A Demonstration of Ocean Acoustic Tomography, Nature, **299**:121-125. (1982).

Okujima M., S. Ohtsuki and H. Hachiya : An estimation Method of Vertical Sound Speed Profiles in Kuroshio Stream by Measuring Sound Transmission Time, IEICE Technical Report, U85-30, **85**:51-56. (1985). (in Japanese)

Rossby T. : On Monitoring Depth Variations of the Main Thermocline Acoustically, J. Geophys. Res., **74**(23):5542-5546. (1969).

Spiesberger J.L., R.C. Spindel and K. Metzger : Stability and Identification of Ocean Acoustic Multipaths, J. Acoust. Soc. Am., **67**:2011-2017. (1980).

Spindel R.C. : An Underwater Acoustic Pulse Compression System, IEEE Trans. Acoust., Speech and Sig. Proc., ASSP-**27**:723-728. (1979).

Spindel R.C. and J.L. Spiesberger : Multipath Variability due to the Gulf Stream, J. Acoust. Soc. Am., **69**:982-988. (1981).

Taira K. and T. Teramoto : Path and Volume Transport of the Kuroshio Current in Sagami Bay and their Relationship to Cold Water Masses near Izu Peninsula, J. Oceanogr. Soc. Japan, **42**:212-223. (1986).

Thorp W.H. : Analytic Description of the Low Frequency Attenuation Coefficient, J. Acoust. Soc. Am., **42**:270-271. (1967).

Watts D.R. and H.T. Rossby : Measuring Dynamic Heights with Inverted Echo Sounders : Results from Mode, J. Phys. Oceanogr., **7**(3):345-358. (1977).

Wenz G.M. : Acoustic Ambient Noise in the Ocean, Spectra and Sources, J. Acoust. Soc. Am., **34**:1936-1956. (1962).

Wunsch C. : Determination the General Circulation of the Oceans, A Preliminary Discussion, Science, **196**:871-875. (1977).

Wunsch C. : The General Circulation of the North Atlantic West of 50W Determined from Inverse Methods, Rev. Geophysics and Space Physics, **16**:583-620. (1978).

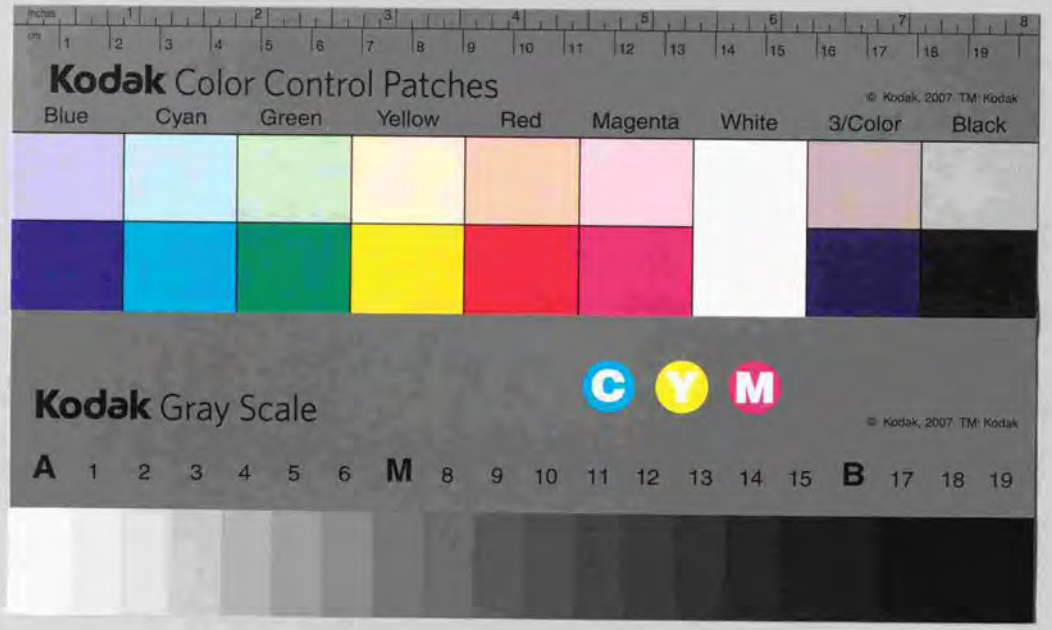
Kodak Color Control Patches
© Kodak, 2007 TM: Kodak
Blue
Cyan
Green
Yellow
Red
Magenta
White
3/Color
Black
Kodak Gray Scale
C
Y
M
© Kodak, 2007 TM: Kodak
A 1 2 3 4 5 6 M 8 9 10 11 12 13 14 15 B 17 18 19